OPEN ACCESS

University of BRISTOL

Sheehan, H. M., Traiger, E., Poole, D. J., & Landberg, L. (2022). Predicting Linearised Wind Resource Grids using Neural Networks. *Journal of Wind Engineering and Industrial Aerodynamics*, *229*, [105123]. https://doi.org/10.1016/j.jweia.2022.105123

Publisher's PDF, also known as Version of record

License (if available):
CC BY

Link to published version (if available):
10.1016/j.jweia.2022.105123

Link to publication record in Explore Bristol Research
PDF-document

This is the final published version of the article (version of record). It first appeared online via Elsevier at https://doi.org/10.1016/j.jweia.2022.105123.Please refer to any applicable terms of use of the publisher

University of Bristol - Explore Bristol Research
General rights

This document is made available in accordance with publisher policies. Please cite only the published version using the reference above. Full terms of use are available:
http://www.bristol.ac.uk/red/research-policy/pure/user-guides/ebr-terms/

Journal of Wind Engineering & Industrial Aerodynamics 229 (2022) 105123

Contents lists available at ScienceDirect

Journal of Wind Engineering & Industrial Aerodynamics

journal homepage: www.elsevier.com/locate/jweia

Predicting Linearised Wind Resource Grids using Neural Networks

Helen Sheehan [a,b,*], Elizabeth Traiger [c,1], Daniel Poole [b], Lars Landberg [d]

[a] Cabot Institute, University of Bristol, UK
[b] School of Civil, Aerospace and Mechanical Engineering, University of Bristol, UK
[c] DNV, NO
[d] DNV Denmark, DK

ARTICLE INFO

Keywords:
Wind Resource Assessment
Machine Learning
Grid-Kernel Neural Networks
Deep Neural Networks
Convolutional Neural Networks
WAsP

ABSTRACT

Modelling the flow over terrain is a key element of wind resource assessments within the wind energy industry. Existing flow modelling methods range from fast, low fidelity analytical models to time-consuming and computationally expensive high-fidelity Computational Fluid Dynamics (CFD) software. In this work, a *Grid-Kernel Neural Network* approach has been developed and used to create surrogate models to emulate the WAsP wind resource software, by calculating the changes in wind speed and direction due to the orography and roughness of terrain. This data-driven approach has proven to be successful in predicting the orographic speed and direction changes at multiple heights above ground. At 100 m above ground, the mean absolute error values were 1.6% speedup and 0.4° for the orographic speed and direction changes, respectively. Although the WAsP model is a linear, potential flow solver, the findings here can be counted as a first step towards creating a fully data-driven CFD wind resource model.

1. Introduction

When deciding on an appropriate location to situate a wind farm, a developer must obtain an estimate of the energy which the wind farm could produce. To do this, the wind resource over the potential sites must be calculated, as the elevation and terrain characteristics affect the speed and direction of the wind. A variety of flow modelling options are available for calculating this wind resource, ranging from fast, low-fidelity engineering models (Jensen, 1983; Frandsen et al., 2006) to high-fidelity but computationally expensive CFD software (Song et al., 2014; Bleeg et al., 2018; Navarro Diaz et al., 2019). Time and computational power constraints can make engineering flow models more attractive than full CFD. Interest in the use of artificial intelligence in industrial applications is gaining momentum (Kareem, 2020), and the wind energy industry in particular is investigating the use of data-driven modelling to enhance or even replace current explicitly physics-driven methods, such as blade loading calculation (Lalonde et al., 2021) or damage detection (Regan et al., 2017), power production optimisation (van der Hoek et al., 2020) and wind field reconstruction (Zhang and Zhao, 2021) or speed prediction (Sharma et al., 2020). Recently, investigations have been undertaken into applying data-driven methods specifically to wind speed or resource calculation, such as k-nearest neighbours approaches to predicting wind speeds from terrain in Quiroga-Novoa et al. (2021) and Lee et al. (2022), and the coupling of numerical weather prediction models with neural networks for wind speed forecasting by Donadio et al. (2021). When appropriately designed and trained, these data-driven models can perform complex calculations more efficiently and with comparable accuracy to the white-box models they have been trained on, for example the MeshGraphNets model of Pfaff et al. (2020). This makes them desirable as surrogate[2] models for applications such as CFD.

In this work, machine learning models for the calculation of changes in wind speed and direction over terrain have been created and their performance evaluated. The Wind Atlas and Analysis Program (WAsP) (DTU Wind Energy, 2022) has been used as the target model on which the data-driven models were trained. While WAsP is a lower-fidelity model than iterative CFD methods that solve the flow equations, it is an industry-standard approach for determining the wind resource over terrain, and its fast running times allow for the generation of training data for a range of wind directions and a variety of terrains. The approach developed here is a fast, grid-based neural network model that provides estimates of the wind resource over a given terrain with fidelity comparable to that of WAsP. This work can be seen as a first step towards fully data-driven CFD for wind resource calculations, which would be especially important for evaluating wind resource from

* Corresponding author at: School of Civil, Aerospace and Mechanical Engineering, University of Bristol, UK.
E-mail address: helen.sheehan@bristol.ac.uk (H. Sheehan).
[1] Dr. Elizabeth Traiger's present address is: DNV Energy USA, Inc., Seattle, USA
[2] *Surrogate model* here meaning a data-driven model that uses the same inputs and produces comparable outputs to a target model.

https://doi.org/10.1016/j.jweia.2022.105123
Received 14 April 2022; Received in revised form 2 August 2022; Accepted 3 August 2022
Available online 5 September 2022
0167-6105/© 2022 The Authors. Published by Elsevier Ltd. This is an open access article under the CC BY license (http://creativecommons.org/licenses/by/4.0/).

Acronym

AGL	Above Ground Level
B-Z	Bessel expansion on a Zooming grid
CFD	Computational Fluid Dynamics
CNN	Convolutional Neural Network
DNN	Deep Neural Network
GKNN	Grid-Kernel Neural Network
MAE	Mean Absolute Error
MSE	Mean Squared Error
ReLU	Rectified Linear Unit
std. dev.	standard deviation
WAsP	Wind Atlas and Analysis Program

a range of directions, or wind farm layout optimisation, both of which require multiple flow calculation instances. Outside of wind resource calculations, a fast and accurate data-driven CFD model would be useful for the prediction of wind fields in a wind farm for e.g. wind farm control (Kheirabadi and Nagamune, 2019) or power prediction (Howland and Dabiri, 2019).

This paper is organised as follows: Section 2 outlines the target model and the machine learning methods used; Section 3 outlines the data, the models' inputs, and the evaluation techniques; Section 4 details the Convolutional Neural Networks tested; Section 5 describes the development of and results from the novel Grid-Kernel Neural Networks; finally, Section 6 details the conclusions made.

2. Methodology

When designing data-driven surrogates for physics-based models, consideration must be given to the form of the target model, in this case the WAsP software; this informs the choice of machine learning techniques employed in the surrogate models.

2.1. WAsP

WAsP is an industry-standard software for modelling the air flow over terrain, based on the European Wind Atlas (Troen and Lundtang Petersen, 1989). WAsP uses a linear potential sub-model to calculate the changes in wind speed and direction due to elevation, and a separate sub-model for the effects of changes in terrain roughness on the wind speeds. WAsP produces two-dimensional grids of the wind resource at a user-specified height[3] Above Ground Level (AGL). Each of the wind resource variables is calculated for a range of constant wind directions determined by the number of wind sectors chosen, and are reported as dimensionless values that do not depend on the incoming wind speed. The WAsP model has known limitations, such as requiring shallow slopes in the terrain being analysed to satisfy the assumption that the flow remains attached. From this point, the changes in wind speed are referred to as *speedup*, the changes in wind direction are known as *turn*, and the terms *elevation* and *height* refer to terrain orography and the vertical distance of the wind resource map AGL respectively.

The orographic sub-model of WAsP is based on the B-Z (Bessel expansion on a Zooming grid) model of Troen (1990) (which was developed from Jackson and Hunt's model for air flow over a low hill (Jackson and Hunt, 1975)) and calculates perturbations in the wind velocity induced due to changes in elevation on a polar grid with increasing radial spacing between grid points from the centre outwards (a "zooming" grid) applied over the terrain. This model also takes the roughness of the terrain into account, by applying an appropriate factor to the orography-induced wind speed changes. The orographic speedup is calculated as the ratio of the wind speed over the orography to the wind speed over a flat terrain; the orographic turn is calculated as the change in wind direction from the incoming wind direction.

The roughness sub-model of WAsP calculates the effect of changes in the type of terrain on the wind speed. The transitions between areas of different roughness lengths introduce turbulence into the flow at (approximately) ground level, initiating an internal boundary layer, giving a new wind profile which propagates vertically upwards with distance downstream from the roughness change. WAsP assumes a logarithmic wind speed profile, and uses the roughness lengths, the number of roughness transitions in a given direction, and the meso-scale roughness (meso-roughness) to calculate changes in wind speed. The meso-roughness is calculated at each grid point over the terrain using a weighted sequence of the roughness changes upstream, ensuring that more distant roughness changes have less influence on the flow at the current location. From this, the equilibrium surface roughness to which the geostrophic drag law applies is found, which is the meso-roughness for the current grid point. The speedup due to roughness is the ratio of the wind speed at each point on the grid to the wind speed at those points if the terrain had a single meso-scale roughness length.

Jackson and Hunt (1975) compared the results of their linear potential model for flow over a low hill against experimental data from both wind tunnels and real terrain, and confirmed a reasonable match between their calculated speedup factor and the measurements. After incorporating Jackson and Hunt's model into WAsP, Walmsley et al. (1990) also conducted a series of comparisons of various wind resource models (including WAsP) and observations from Blashaval Hill in Scotland, and found that for most wind directions the error in wind speed from WAsP was less than 7%. More recent validation of the WAsP model in Bowen and Mortensen (2004) showed that the errors in mean wind speeds are between $\pm 2\%$ for a range of sites, which is a good agreement. However, this work also suggested the use of a ruggedness index to quantify whether the elevation of a given site is too steep to be within the WAsP performance envelope, as the lack of modelling of separated flow in WAsP can cause errors when predicting the wind resource over such terrain. For the WAsP 11 version used in this paper, the report by Mortensen (2016) recommends that WAsP's flow modelling errors for both horizontal and vertical extrapolation are between 0 and 5% of the wind speed. Byrne et al. (2021) compared WAsP 11 to LiDAR-measured data for a single wind turbine, with errors in the mean wind speeds of mostly less than 7.5%, but were very dependent on the height of the LiDAR and heavily affected by surrounding buildings.

2.2. Machine learning

There is an extensive array of research into the use of machine learning for fluid dynamics simulations, using many different types of data-driven models from random forests (Ladický et al., 2015) to neural networks (Lee and You, 2019). Deep Neural Networks (DNNs) are interconnected nets of trainable "neurons", each of which has a weight value; these neurons are usually organised into layers, each of which has a bias value. These weights and biases can be optimised, e.g. by supervised learning where the network aims to produce outputs as close to known values as possible, given specific input data. DNNs are typically fully-connected and feed-forward, meaning that each neuron in a layer is connected to all neurons in the layers before and after it, and that all of these connections pass information "forwards" (from the inputs towards the outputs), and no information is passed "backwards". Such machine learning models can be tuned through the choice of architecture, activation functions, optimiser, and other hyperparameters.

[3] This height follows the terrain, to predict the wind resource at the hub heights of turbines placed at any point on the terrain.

To emulate the WAsP model, surrogate models would be required to take in two-dimensional grids of terrain data (i.e. elevation, roughness) and produce two-dimensional grids of the wind resource over this area. Similarities were drawn between this task and image processing, particularly data-driven image transformation models, as seen in Isola et al. (2016). These are usually Convolutional Neural Networks (CNNs), which convolve iteratively learned filters over channels of image data to produce multiple feature layers, gradually transforming the image data. Several papers have employed CNNs for flow field prediction, with the calculation of flow around an aerofoil being a popular test case. Both Bhatnagar et al. (2019) and Thuerey et al. (2020) created CNN-based autoencoder networks to predict the steady-state velocity and pressure fields around aerofoils, given the free stream conditions and shape of the aerofoil as inputs, provided as a combination of data grids and single numerical values. In another application of CNNs, Lee and You (2019) used this type of network as both generator and discriminator in a generative adversarial network for predicting the time-varying velocity and pressure flow fields around a cylinder, inspired by video processing networks.

An inevitable consequence of using black-box models such as neural networks is the lack of transparency of the workings of the model, potentially making it challenging to quantify their limits or prove their reliability. Raissi et al. (2019) incorporated the physical equations of training data sets into their DNNs through custom loss functions in the training stage. These loss functions constrained the DNN to learn the appropriate boundary conditions and constraints in order to reliably determine correct equations, e.g. learning the Navier–Stokes equations for a fluids data set. Including the physical basis in a data-driven surrogate model in this way provides greater confidence to the designers and users that the network has learned valid relationships between the input and output data, as well as needing fewer input–output data pairs to learn these mappings and hence train the model (as proven in Raissi et al. (2019)).

After reviewing existing work on machine learning models for image transformation and fluid dynamics, the spatial transformation abilities of CNNs were clearly advantageous when handling grid-based data. From this, Sections 3 and 4 detail the investigations carried out into the use of CNNs as WAsP surrogate models.

3. Model set-up

Separate surrogate models for the orographic speedup, orographic turn and roughness speedup sub-models of WAsP were developed in this work. All neural networks described were built with the PyTorch package.

3.1. Site data

Elevation and roughness input files were obtained for a number of real sites, and the computer-generated Waspdale site included in the WAsP 11 installation was added to the real training sites. Sites were selected to give a diverse set of topographical features including lakes, hills, valleys, and mountainous and flat areas. The terrains of sites used for training and inference are given in Appendix A; Table 1 gives a summary of their elevations and roughness lengths. The wind resource maps were calculated at heights of 10 m and 100 m AGL, with a grid resolution of 50 m in both the x and y directions, using the WAsP 11 software. Of the twelve direction sectors calculated for each site, nine were used for training, two for validation, and one was held back for final, blind testing (see Section 5.4).

Table 1
Site topography summary.

Site	Elevation (m)			Roughness length (m)		
	Minimum	Mean	Maximum	Minimum	Mean	Maximum
1	100	178	350	0.0	0.029	0.030
2	710	786	910	0.0	0.048	0.35
3	785	849	924	0.0	0.011	0.30
4	839	919	960	0.0	0.027	0.50
5	500	808	1050	0.001	0.086	0.30
6	695	750	805	0.0	0.010	0.30
7	−4	9	32	0.0	0.30	1.5
8	360	431	766	0.0	0.23	0.30
9	620	661	700	0.0	0.020	0.35
10	585	650	692	0.0	0.024	0.35
11	180	200	230	0.0	0.088	0.50
12	176	453	720	0.0	0.037	0.50
13	825	896	951	0.0	0.010	0.50
14	570	592	685	0.0	0.045	0.50

3.2. Inputs

For the orographic speedup and turn models, the terrain elevation is evidently a key input, and roughness is also included in the WAsP calculations. Hence, the machine learning models investigated here used combinations of the terrains' elevation, elevation gradients and roughness as inputs. To incorporate directional information into the inputs, the elevation gradients were transformed into their components parallel and perpendicular to the wind direction. The roughness lengths over the training sites varied between 0.0 m (i.e. water) and 1.5 m (e.g. for tall trees), the elevation gradient values ranged between approximately ±1.0, and the elevation ranged from around −4 m to 1050 m (see Table 1). The elevation gradients were calculated via first order central difference over the grid spacing in both x and y directions, with first order forward or backward differences as required at the grid edges. To prevent model bias towards the larger inputs, the elevation values were normalised using the min–max technique:

$$z_{mm} = \frac{z - z_{min}}{z_{max} - z_{min}} \tag{1}$$

where z represents elevation, z_{mm} is the normalised elevation, and the minimum (z_{min}) and maximum (z_{max}) elevations were determined over all sites used for training. The range of normalised elevation values was then between ±1.0, giving a similar range of values for each of the three input variable types. Where wind direction was included as a model input, it was also normalised to between 0.0 and 1.0 via:

$$d_{norm} = \frac{d}{360} \tag{2}$$

where d is the wind direction in ° and d_{norm} is the normalised wind direction.

As described in Section 2.1, the roughness speedup is dependent on the roughness, meso-roughness and number of roughness changes in a given terrain area. While the roughness and meso-roughness lengths ranged between 0.0 m and 1.5 m, roughness changes are integer numbers of transitions "seen" by the wind in a given direction, and can be up to 10 transitions per direction sector. Similar to the normalisation of the elevation inputs for the orographic speedup models, the roughness and meso-roughness lengths were transformed to have similar magnitudes to the number of roughness changes, to prevent any bias towards one type of input. Based on the equations of the roughness speedup sub-model in Troen and Lundtang Petersen (1989), the roughness and meso-roughness were transformed to:

$$r_t = \ln\left(\frac{1}{r}\right) \tag{3}$$

where r is the roughness or meso-roughness, and r_t is the transformed value. Additionally, the difference between these transformed values was included as an input in some cases (specified in the descriptions of the models).

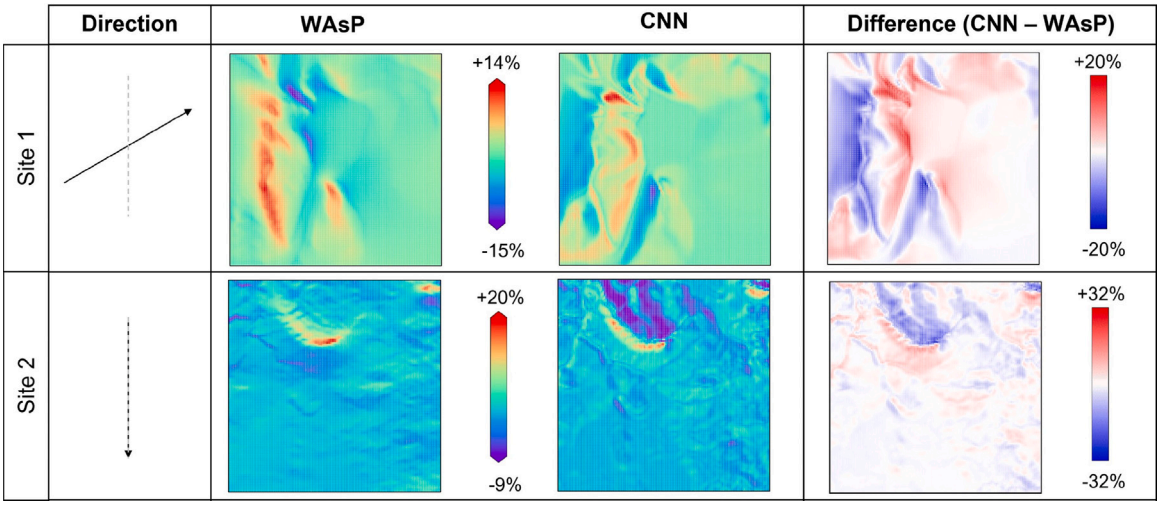

Fig. 1. Results from the most promising Convolutional Neural Network for predicting orographic speedup at 100 m AGL; for (top–bottom) Sites 1 & 2, shows (left–right): WAsP calculated speedup; CNN predicted speedup; difference (CNN-WAsP). Speedup values and differences are given in % speedup; speedup colour scales are based on WAsP outputs. (Note that the Site 1 data shown here was part of the training data rather than the validation data, but is included here for consistency.).

Table 2
Error metrics for the orographic speedup GKNN models when compared to WAsP. All errors in % speedup.

Height (m AGL)	MAE	Error std. dev.	Minimum error	Maximum error
10	1.90	2.79	−51.3	48.4
100	0.652	1.04	−14.7	14.6

Table 3
Error metrics for the orographic turn GKNN models when compared to WAsP. All errors in ° clockwise turn.

Height (m AGL)	MAE	Error std. dev.	Minimum error	Maximum error
10	0.898	2.43	−179	180
100	0.397	0.635	−11.9	10.3

Table 4
Error metrics for the roughness speedup GKNN models when compared to WAsP. All errors in % speedup.

Height (m AGL)	MAE	Error std. dev.	Minimum error	Maximum error
10	0.768	1.45	−23.0	24.1
100	0.517	0.980	−10.8	8.80

Table 5
Error metrics for inference on the final GKNN models compared to WAsP.

Height (m AGL)	MAE	Error std. dev.	Minimum error	Maximum error
Orographic speedup (% speedup)				
10	3.68	7.04	−103	111
100	1.64	3.01	−31.1	23.8
Orographic turn (° turn)				
10	1.39	3.09	−179	176
100	0.446	0.786	−9.77	9.50
Roughness speedup (% speedup)				
10	0.472	1.16	−18.2	25.2
100	0.384	0.953	−9.91	11.7

3.3. Performance metrics

To compare the performance of the different surrogate models tested, the output maps produced by each model were evaluated. Several statistical metrics were calculated, including the minimum and maximum error, the Mean Absolute Error (MAE):

$$\mathrm{MAE} = \frac{1}{N}\left(\sum_{i=1}^{N} |\hat{v}_i - v_i|\right) \tag{4}$$

and the standard deviation (std. dev.) of errors:

$$\text{std. dev.} = \sqrt{\frac{1}{N}\left(\sum_{i=1}^{N} |(\hat{v}_i - v_i) - \mu_e|^2\right)} \tag{5}$$

where N is the total number of output points, $\hat{v}_i$ is the surrogate model-predicted speedup or turn at a single coordinate, v_i is the equivalent WAsP calculated speedup or turn, and μ_e is the average error. Hence, for a set of output wind resource grids produced by a data-driven model, the MAE is the sum of the absolute differences between the WAsP-calculated and predicted resource value (speedup or turn) at each coordinate, divided by the number of coordinate points evaluated. The standard deviation is calculated by assuming that the differences between the WAsP and data-driven values over all coordinates can be fitted to a normal distribution. The results presented in Tables 2–5, described later in the paper, are calculated over all coordinate points for the validation (or inference) sites and directions considered. While it is difficult to evaluate two-dimensional data using single numbers, these metrics are useful for defining the spread of errors, and diagnosing where the models are generally under- or over-predicting.

Note that the model outputs plotted here and error metrics presented represent the validation data, unless otherwise specified.

4. Convolutional Neural Networks

Following the review of existing research on machine learning for fluid dynamics in Section 2.2, the initial tests into creating surrogate wind speedup models over terrain used CNNs in autoencoder-style architectures, based on those of Bhatnagar et al. (2019) and Thuerey et al. (2020), with small filter sizes relative to the input grids.

4.1. Orographic speedup results

Using autoencoder-style CNNs to predict the orographic speedup over a terrain did not produce successful results, even after testing a range of model hyperparameters such as filter size, number of network layers, number of feature channels and combinations of input variables. The most promising results are shown in Fig. 1. The speedups produced by this CNN were heavily influenced by the dominant elevation

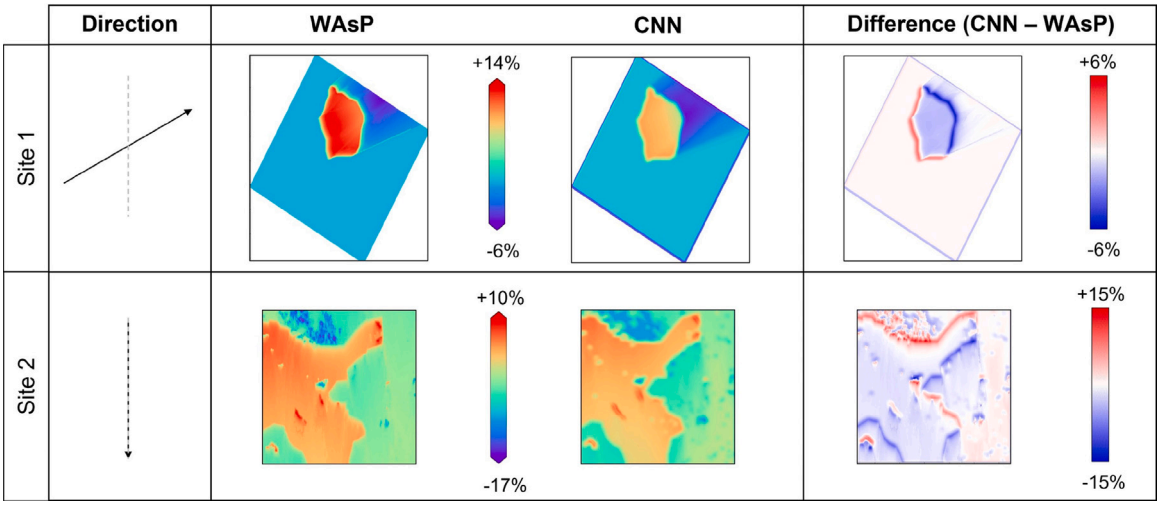

Fig. 2. Results from the most promising Convolutional Neural Network for predicting roughness speedup at 10 m AGL; for (top–bottom) Sites 1 & 2, shows (left–right): WAsP calculated speedup; CNN predicted speedup; difference (CNN-WAsP). Speedup values and differences are given in % speedup; speedup colour scales are based on WAsP outputs.

features, such as the hill in Site 2. However, the more complex and detailed changes in the wind speed due to more gradual changes in the elevation (e.g. the hill and valley slopes in Site 1) were not captured. Following on from the initial CNN surrogate models, a U-Net (Ronneberger et al., 2015) style CNN architecture was investigated; the U-Net structure is a modified form of an autoencoder network, with "skip" connections between corresponding encoder and decoder layers. These connections give the network an ability to "remember" input data even in deeper layers, which was theorised to be similar to the relation between orographic speedup and terrain elevation, but these models were unsuccessful.

A possible reason for the lack of success here could be the comparatively small number of sites that were available. For context, the U-Net style aerofoil flow model of Thuerey et al. (2020) was trained on ~27,000 sets of simulation data; this compares to ~250 different maps of each output variable available here. Classic image processing data augmentation techniques such as "zooming" or rotating were not possible here as these would require the input and output data to be re-calculated in WAsP to ensure physical feasibility. In total around 250 CNN architectures and training data combinations were tested for predicting orographic speedup at various heights.

4.2. Roughness speedup results

In the same vein, a range of CNNs were tested to predict roughness speedup grids. The filter sizes used were relatively small compared to the grid size (as in Bhatnagar et al. (2019)), and the number of layers, channels and filters were investigated. The most promising CNN results for roughness speedup are seen in Fig. 2 for 10 m AGL; note that in this CNN, the input grids were rotated such that the incoming wind direction was always 0°. Results from 10 m AGL are shown in this section rather than 100 m AGL as these were the best performing cases out of models trained at each height. This model was able to scale the outputs to the correct range of speedup values, but did not learn to apply the changes in wind speed downstream of roughness transitions. This was exacerbated in the tests at 100 m AGL, with most of the CNNs collapsing and unable to generate output grids that varied significantly from the input grids. As with the orographic speedup CNNs, the comparatively small training data set could be a significant factor in the lack of success with this approach. In total around 100 CNN architectures and training data combinations were tested for predicting roughness speedup at various heights.

5. Grid-Kernel Neural Networks

From the tests detailed above, training CNNs in an autoencoder architecture on WAsP orographic and roughness speedups did not produce accurate or robust surrogate models. A new approach, called the Grid-Kernel Neural Network (GKNN), was therefore developed, and is presented here. A schematic of the GKNN approach is shown in Fig. 3, with the steps being:

1. From terrain elevation and roughness maps, calculate the elevation gradients via finite difference and the wind resource and associated parameters with WAsP;
2. (a) Take in maps of relevant input and output data;
   (b) Split these maps into as many sub-grids (or *kernels*) of a specified size (e.g. 15 × 15 grid points for inputs, single point for output) as possible;
3. Use a given pattern of points from each kernel, as well as information such as wind direction, as inputs and target outputs for training a fully-connected, feed-forward Deep Neural Network.

The kernels in this GKNN approach are analogous to filters in a CNN, but with a direct connection between the size of the kernels applied to the input variables and the output values produced by the network. Finding the optimum sub-grid size applied to a particular input in a GKNN could be interpreted as the radius of influence of that input variable on the output, e.g. the radius of influence of the elevation on a single orographic speedup point. This optimal kernel size was intended to inform filter sizes in CNNs, in addition to being a generally useful finding.

5.1. Orographic speedup results

To determine an optimal input kernel size for calculating orographic speedup values, a series of GKNN tests were completed with varying input sub-grid sizes and a single output point, with all other parameters (training data, number of neurons and layers, activation functions, optimiser and loss function) kept the same. Fig. 4 shows the results of these tests for Site 1 at 100 m AGL, using either the normalised elevation or the elevation gradient components parallel to the wind as input (as well as the normalised wind direction). The smallest input kernel sizes lacked the capacity to transform the shapes of the input maps, but did scale the values to match the orographic speedup magnitudes. At the largest input sub-grid sizes in Fig. 4, the optimum size had been surpassed, and the model outputs began to break down into noise. However, at the optimum kernel size of around 1.2 km

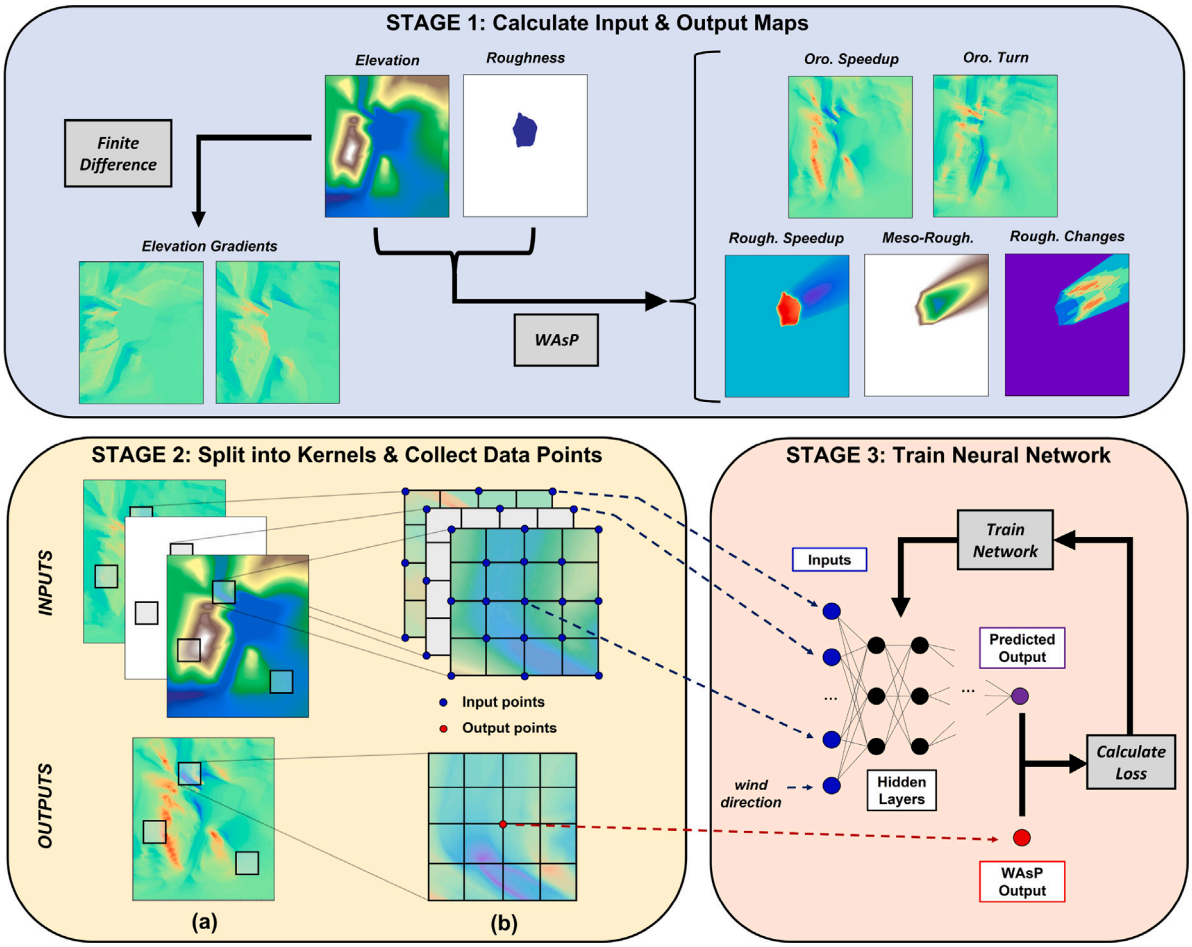

Fig. 3. Flow chart of the Grid-Kernel Neural Network process. Stage 1 (top): input and output map calculation. Stage 2 (bottom left): (a) splitting maps into kernels; (b) taking data points from kernels. Stage 3 (bottom right): training a Deep Neural Network. "Oro." and "Rough." are shorthand for "Orographic" and "Roughness" respectively.

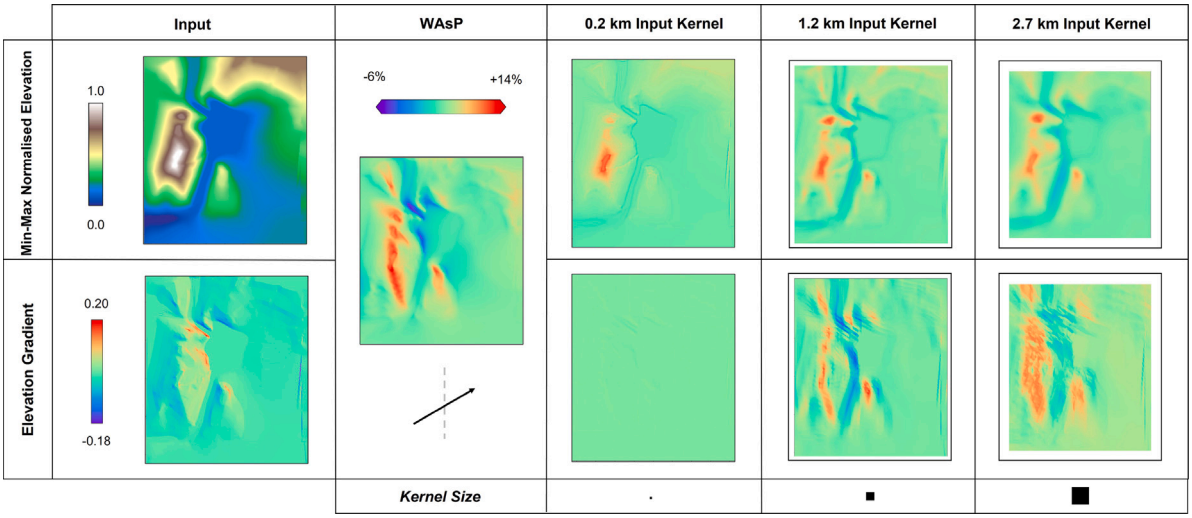

Fig. 4. Comparison of input kernel sizes for GKNN models predicting orographic speedup at 100 m AGL, using (top) min–max normalised elevation or (bottom) the component of elevation gradient parallel to the wind direction as inputs, and using data from Site 1 only. From left to right: input maps; target output map; GKNNs with 0.2 km square input kernel; GKNNs with 1.2 km square input kernel; GKNNs with 2.7 km square input kernel. Speedup values are in % speedup; speedup colour scales are based on WAsP outputs.

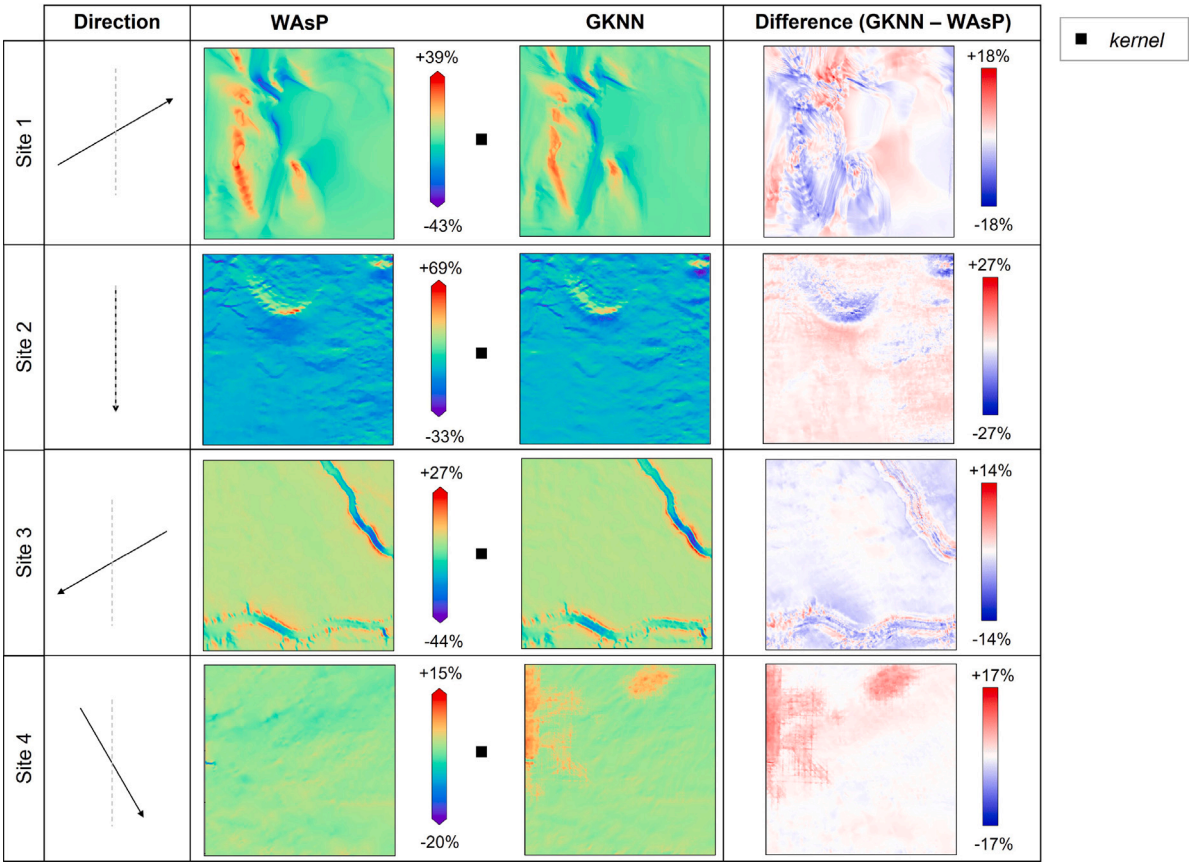

Fig. 5. Results from the final GKNN model for predicting orographic speedup at 10 m AGL; for (top–bottom) Sites 1–4, shows (left–right): WAsP calculated speedup; GKNN predicted speedup; difference (GKNN-WAsP). All speedup and difference values are in % speedup; speedup colour scales are based on WAsP outputs.

side length, using elevation gradient as input, the model had sufficient information (despite having a sparse pattern of points from the input kernel) to give recognisable predictions of the orographic speedup in terms of both shape and scale across the whole terrain.

Using this GKNN approach and kernel size of 1.2 km, a comprehensive set of investigations into the input combinations, DNN architectures, training epochs and methods to augment the training data were carried out, but for brevity are not described here.[4] For the final models, separate models were trained on orographic speedup data at 10 m and 100 m AGL, each using a DNN with 500 neurons split over 10 layers, 1-D batch normalisation (Ioffe and Szegedy, 2015) followed by Rectified Linear Unit (ReLU) activation after each layer, and a single output point. Each network used Mean Squared Error (MSE) loss and was trained for between 50 and 60 epochs, stopping at the best epoch, using data from eleven sites (Sites 1–11). The results can be seen in Fig. 5 (the results at 100 m AGL are given in Appendix B), and the error metrics for both heights are given in Table 2. Given that the same model architecture was used for each height, this kernel size and pattern contains enough information to give decent predictions of the orographic speedup at multiple heights. The GKNNs produced WAsP-style orographic speedups with good accuracy over flat, non-complex terrain areas with gradual, small changes in speedup (e.g. MAE of less than 1% speedup for Site 4 shown in Fig. 5), and had reasonable predictions of the speedups in valleys and around hills in terms of both scale and shape. In WAsP, the orography-based speedup (and turn) maps are calculated over zooming, polar grids of points, which is similar to the kernel approach of these GKNN models; this may be a factor in the success of this method.

In some complex terrain areas the model did not achieve the most extreme speedups observed in the target (WAsP) outputs, such as the increase in speed over the tops of hills, and struggled around areas of sharp changes in elevation such as the valley feature in the top right of Site 3 in Fig. 5. The effect of the valley edges on the surrounding speedups were seen in the model predictions, but not in the WAsP speedup map; these sharp changes in elevation seemed to dominate multiple sub-grids taken in their vicinity. Small-scale details were also sometimes "overlooked" by the GKNN model (e.g. around the lower valley of Site 3 in Fig. 5), potentially due to the spacing that exists between adjacent input kernel points. If, similarly to a CNN, a denser pattern of points within a kernel were used as inputs to the DNN of the GKNN (which would require a significant increase in computing power) this might give the surrogate model outputs better resolution. By area, much of the terrain data provided in training was flat and with low roughness lengths, which may be the cause of some overpredicted speedup values over areas of high roughness in otherwise flat terrain (e.g. Site 4 in Fig. 5).

After determining these optimal kernel sizes for GKNNs, more CNNs were trialled using filters of this size. The outputs from these CNNs were inferior to those from the GKNNs, so the CNNs were not investigated further after this point.

5.2. Orographic turn results

As the GKNN models for predicting orographic speedup proved to be successful, a similar approach was used to create surrogate models for the orographic turn. The orographic turn is the deflection of the wind due to the orography of the terrain, e.g. air flowing around hills or following valleys. Firstly, various kernel sizes for the GKNN were tested using single sites at heights of 10 m and 100 m AGL. The

[4] The MSc thesis, Sheehan (2022) presents the details and results of these investigations.

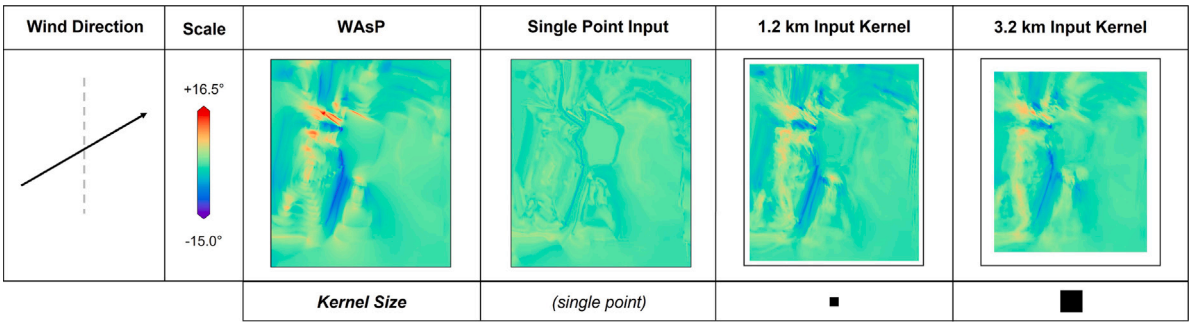

Fig. 6. Comparison of input kernel sizes for GKNN models predicting orographic turn at 10 m AGL, using data from Site 1 only. From left to right: WAsP output; GKNN output with single point input; GKNN output with 1.2 km square input kernel; GKNN output with 3.2 km square input kernel. Turn colour scales are based on WAsP outputs.

inputs for these tests were the normalised wind direction, min–max normalised elevation, elevation gradient parallel to the wind direction, and the roughness; the output was the orographic turn value at the centre of the sub-grid in °. All parameters and settings other than the input kernel size were kept constant. From this investigation (Fig. 6 shows the results for Site 1 at 10 m AGL), the overall optimum kernel size was found to be around 1.2 km side length for both heights, the same as for the orographic speedup GKNN models (Section 5.1). As with the orographic speedup GKNN development, there were some additional investigations into the appropriate GKNN parameters for the final orographic turn models, which are not described here but can be found in Sheehan (2022).

Using the optimal kernel size of 1.2 km, data from Sites 1–11 and the settings described in Section 5.1, a model for predicting the orographic turn at 10 m AGL was trained, with the outputs presented in Fig. 7. These predictions generally showed good matches to WAsP in terms of both scale and shape of the turn maps, with MAE of less than 1°. However there were some areas of error around large orographic features such as the prominent hill in Site 1; by contrast, in Site 4 the errors were relatively uniform across the (flat) terrain. The performance metrics for this model are given in Table 3.

Using this GKNN model at 10 m AGL, there were some outlying large errors in the turn values, as seen in the range of errors in Table 3. The most extreme errors of around ±180° occurred in the site displayed in Fig. 8, in a valley feature to the right hand side of the site. This is a large change in numerical values of the turn but a very small change in the actual wind direction. It is therefore understandable that the model might struggle to predict this sudden change in the direction, given that this discrete jump in values is not present in any of the input maps. There is also a question on how feasible a turn of ±180° in this narrow valley would be in reality. Only one other site (Site 8, Fig. A.8) has errors outside of approximately ±15°, and these are concentrated around a narrow gap between two peaks through which WAsP calculates the flow is turned significantly. The GKNN's tendency to "smooth out" some small-scale flow features may have been the cause of the errors at this site.

A kernel size of 1.2 km side length was used to train a separate GKNN to predict the orographic turn at 100 m AGL, with the same architecture and inputs as for 10 m AGL. The errors for this model (Table 3) were smaller overall than those of the 10 m AGL orographic turn model, which was expected as the terrain has less influence on the flow with increasing height, giving smaller magnitudes of turn. Visually, the orographic turn maps produced by the GKNN were similar to those calculated by WAsP, but the magnitude of the orographic turn was generally slightly under-predicted, with some small areas of high turn not captured in the surrogate model. Given the similarities to the 10 m AGL model, these results have not been included here but are presented in Appendix B.

5.3. Roughness speedup results

Having found an optimal kernel size for orographic speedup and turn GKNN surrogate models, the next stage was to investigate the suitability of the GKNN approach for roughness speedup calculations. Again, a range of input kernel sizes were tested, using the transformed roughness and meso-roughness, number of roughness transitions and the normalised wind direction as inputs, and a single roughness speedup output point; the results of these tests are shown in Fig. 9. At 10 m AGL, the optimal kernel size was found to be around 1.2 km square, which was the same as for the orographic speedups at this height. At 100 m AGL, a larger kernel size of 3.2 km square gave results most closely resembling the ground truth roughness speedups. Given that the effect of a roughness transition on the wind speed propagates vertically upward with downstream distance from the transition, it is sensible for a larger kernel size to be more appropriate for speedups at a greater height above ground. Although not presented here, further experiments with GKNN architectures were carried out and are detailed in Sheehan (2022).

As with the orographic speedup and turn surrogate models, the final GKNN model for roughness speedups at 10 m AGL used an input kernel of 1.2 km square, and a DNN formed of 500 neurons split over 10 layers, with batch normalisation and ReLU activation after each layer, and a single output point. This model was trained using data from seven sites[5] (Sites 1, 2, 4, 5, 7, 8 and 11), for between 50 and 60 epochs, using MSE loss. Note that for consistency, Site 3 is shown in Figs. 10 and 11, and the same validation sectors from Sites 1–11 as for the orographic speedup and turn GKNNs are used to calculate the metrics in Table 4. The inputs to the final model were the normalised wind direction, number of roughness changes, natural log of the inverse of the roughness and meso-roughness, and the difference between these variables. The results from the GKNN for roughness speedup at 10 m AGL are shown in Fig. 10, and the error metrics are given in Table 4. In Fig. 10, the GKNN-predicted roughness speedups for Sites 1–4 were very similar to their WAsP equivalents in terms of form and scale, but the GKNN averaged out some of the detailed areas of high or low speedup, such as those in the top left of Site 4. In the results from Site 1 in particular, it can be seen that the GKNN model learned to apply changes in wind speed downwind of roughness transitions, although in Site 3, this "roughness persistence" was not as pronounced in the GKNN output as in WAsP. However, these results were very promising overall, with good matches between the WAsP and GKNN outputs for a range of terrains, and MAE of less than 1% speedup.

To predict roughness speedups at 100 m AGL, the optimum GKNN configuration found consisted of a kernel size of 3.2 km square, and the same architecture and parameters as for the 10 m AGL model described above. The roughness speedup predictions for Sites 1–4 are shown in

[5] Due to the higher number of input variables, fewer sites could be used compared to training the orographic models.

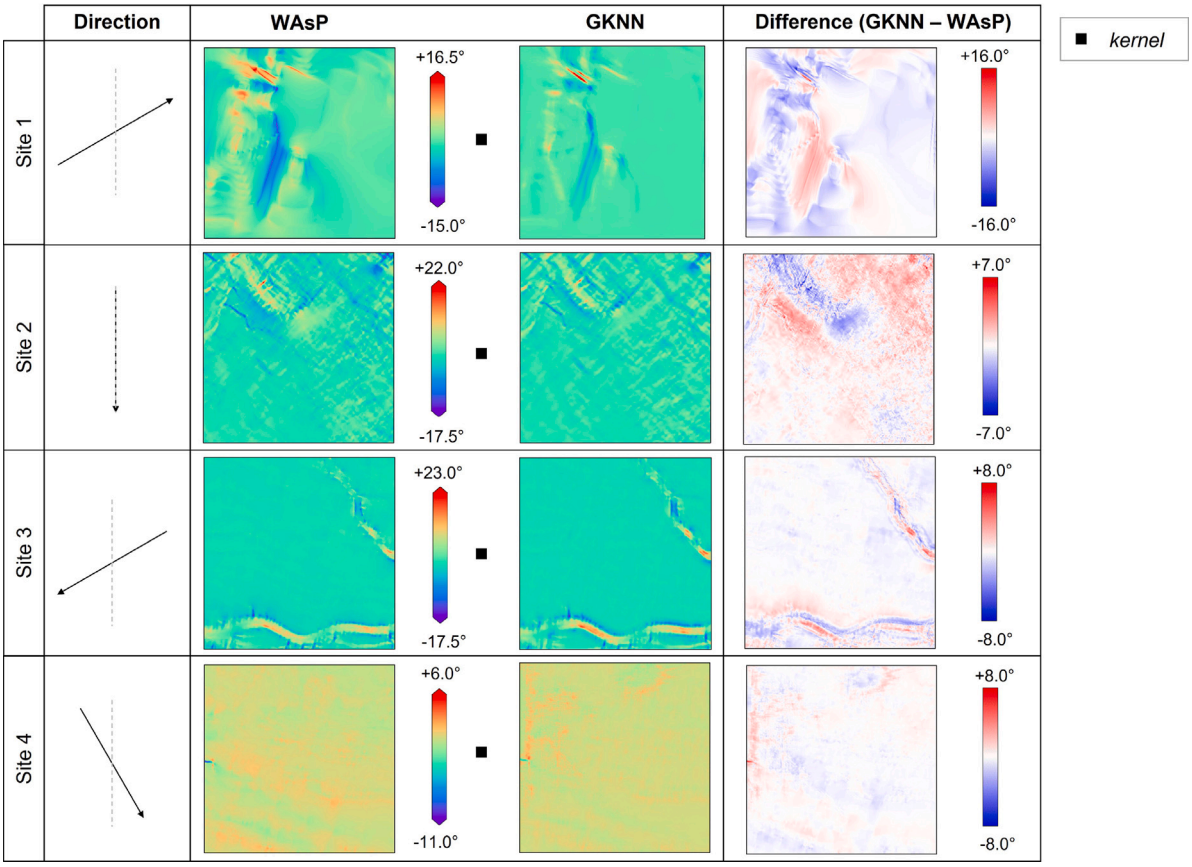

Fig. 7. Results from the final GKNN model for predicting orographic turn at 10 m AGL; for (top–bottom) Sites 1–4, shows (left–right): WAsP calculated turn; GKNN predicted turn; difference (GKNN-WAsP). All turn and difference values are in ° clockwise; turn colour scales are based on WAsP outputs.

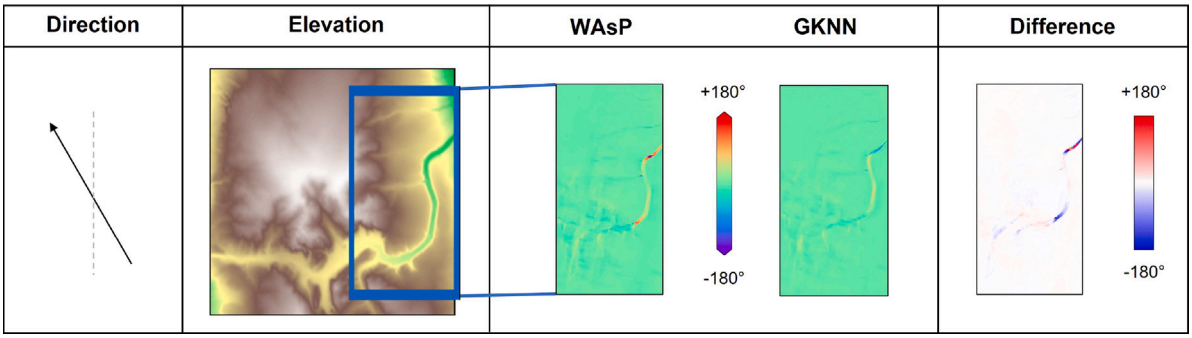

Fig. 8. Orographic turn output from the final GKNN model at 10 m AGL, for Site 5; the detail shown is of a valley with high orographic turn values. Left–right: terrain; WAsP output; GKNN output; difference (GKNN-WAsP).

Fig. 11, and the error metrics are given in Table 4. Most significantly, the area of speed increase due to the effect of the lake in Site 1 was applied at approximately the correct position by the GKNN, which the CNNs (Section 4.2) failed to learn. In Site 2, where the terrain has a much more complex roughness map, the GKNN model produced less believable outputs, but the reason for this remains unclear. In Site 4 the roughness speedups were more significant than the corresponding orographic speedups, as the terrain is relatively flat but has an area of large roughness lengths. This was captured well by the roughness speedup GKNN model, in contrast to the errors in the predictions of orographic speedups over this terrain seen in Fig. 5.

The WAsP roughness sub-model is based on the propagation of an internal boundary layer, which is significantly different to the grid-based orography sub-model. The GKNN method does not resemble WAsP's roughness speedup calculation as strongly as it does the orographic speedup, which is a possible explanation for the difference in performance between GKNN models for roughness and orographic speedup at 100 m AGL.

The roughness speedup GKNN at 100 m AGL was thought to be affected by overfitting, as seen from the loss curves for training and validation in Fig. 12. To prevent overfitting, the commonly used techniques of weight regularisation and dropout were applied to models preceding the final GKNN, with results shown in Fig. 13. From this figure it is evident that neither technique improved on the predictions from the baseline model (i.e. no dropout or weight regularisation), and so these adaptions were not included in the final GKNN model for roughness speedup at 100 m AGL.

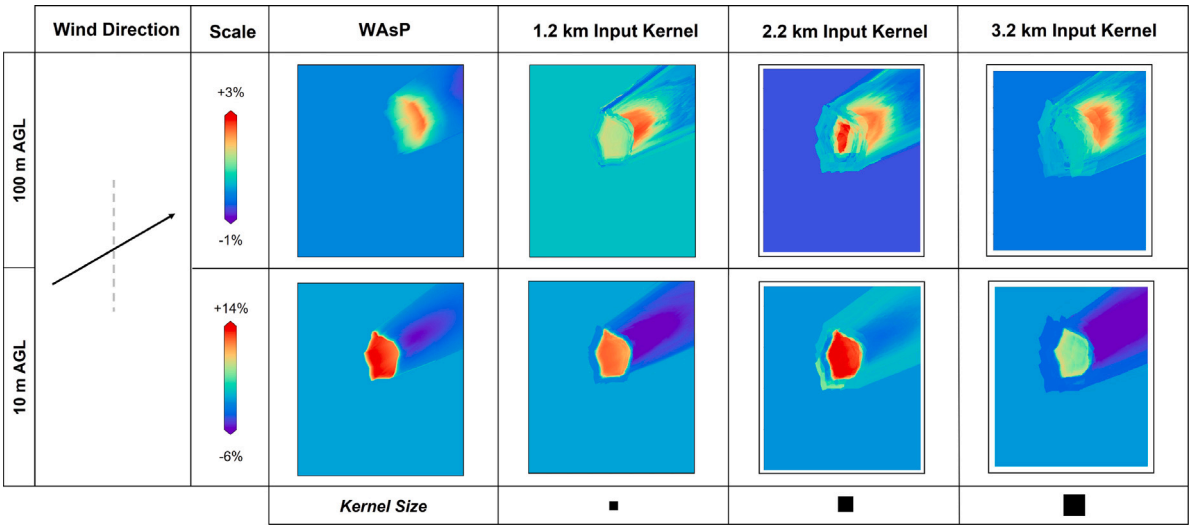

Fig. 9. Comparison of different input kernel sizes for roughness speedup GKNN models at (top) 10 m AGL and (bottom) 100 m AGL. From left to right: WAsP calculated speedups; GKNNs with 1.2 km square input kernel; GKNNs with 2.2 km square input kernel; GKNNs with 3.2 km square input kernel. All speedup values are given in % speedup; speedup colour scales are based on WAsP outputs.

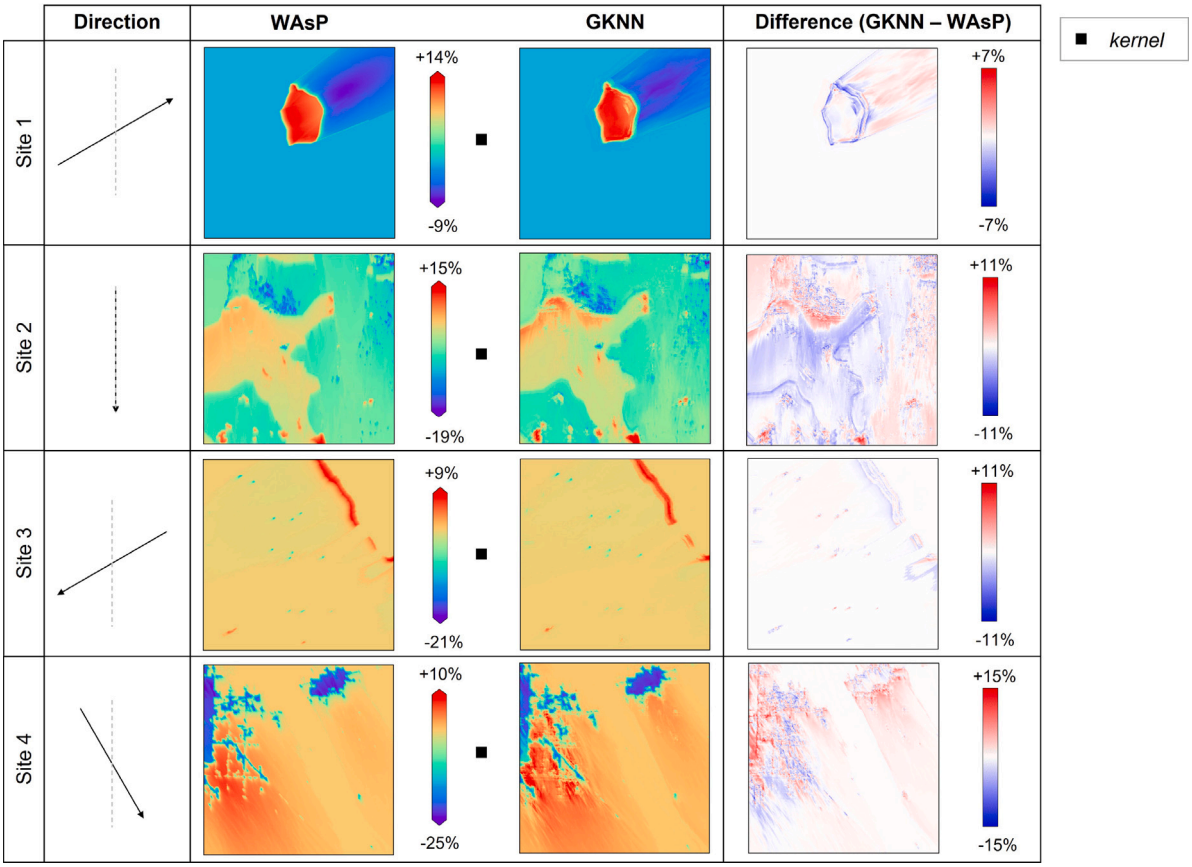

Fig. 10. Results from the final GKNN model for predicting roughness speedup at 10 m AGL; for (top–bottom) Sites 1–4, shows (left–right): WAsP calculated speedup; GKNN predicted speedup; difference (GKNN-WAsP). All speedup and difference values are in % speedup; speedup colour scales are based on WAsP outputs.

5.4. Inference

Once final configurations had been decided for each of the GKNN models by reviewing the outputs and metrics from the validation data sets, inference was undertaken on these surrogate models using data from three new sites. Although one wind direction sector had been held out from each training site for inference, the orographic speedup and turn maps for opposing direction sectors were nearly perfect negatives of each other, and so it was thought to be a better test of the models' capabilities to apply them to previously unseen sites. The sites chosen for

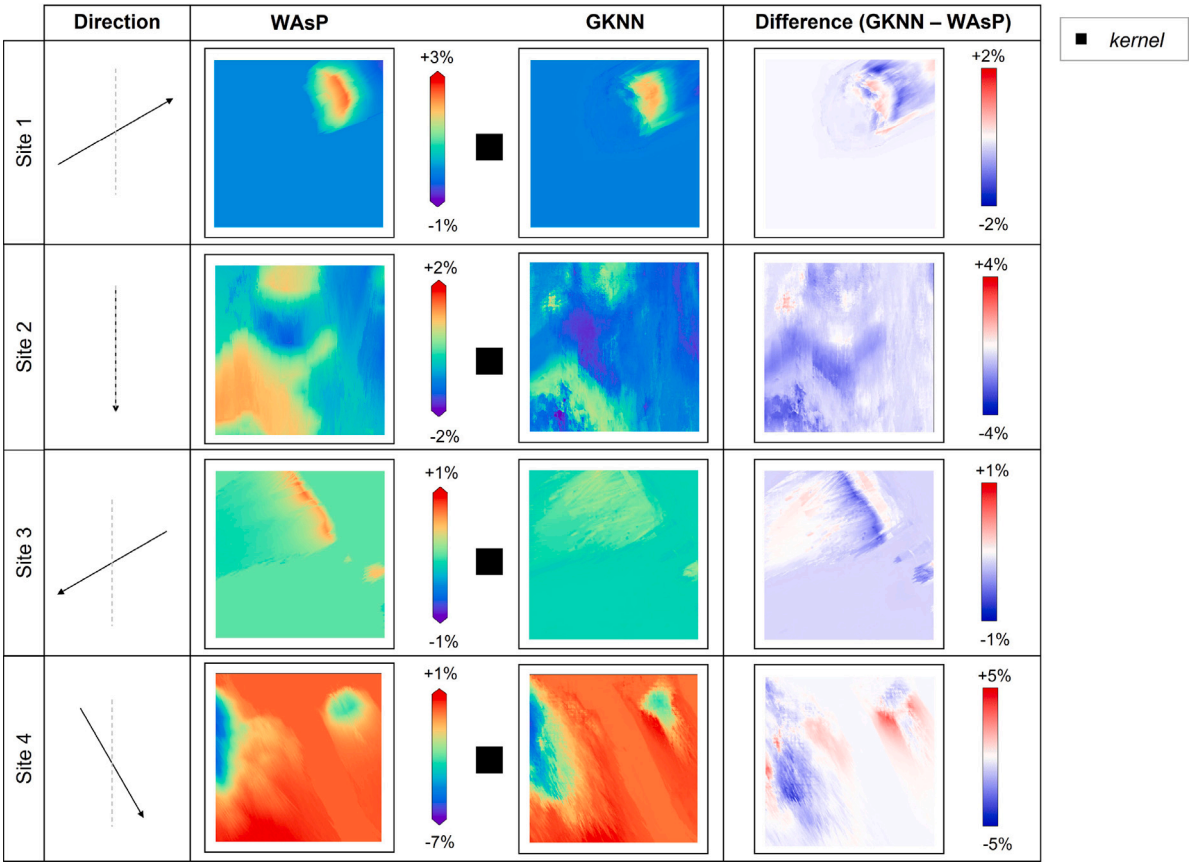

Fig. 11. Results from the final GKNN model for predicting roughness speedup at 100 m AGL; for (top–bottom) Sites 1–4, shows (left–right): WAsP calculated speedup; GKNN predicted speedup; difference (GKNN-WAsP). All speedup and difference values are in % speedup; speedup colour scales are based on WAsP outputs.

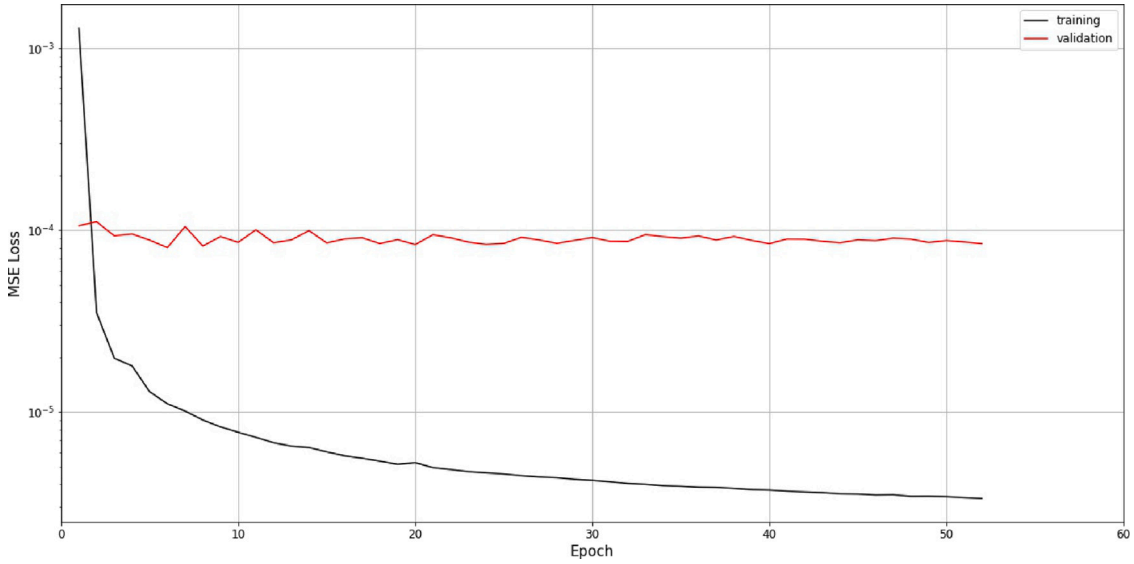

Fig. 12. Loss curves for final GKNN for roughness speedup at 100 m AGL.

these blind tests consisted of a mountainous terrain (Site 12, Fig. A.12), terrain with a single valley feature (Site 13, Fig. A.13), and a flat terrain with significant areas of roughness (Site 14, Fig. A.14). The results for Site 13 for each output variable are shown in Fig. 14 at both 10 m and 100 m AGL, along with the WAsP calculated equivalents. The error statistics are given in Table 5.

The results from the new sites were consistent with the results from validation discussed in Sections 5.1 to 5.3. For the orographic

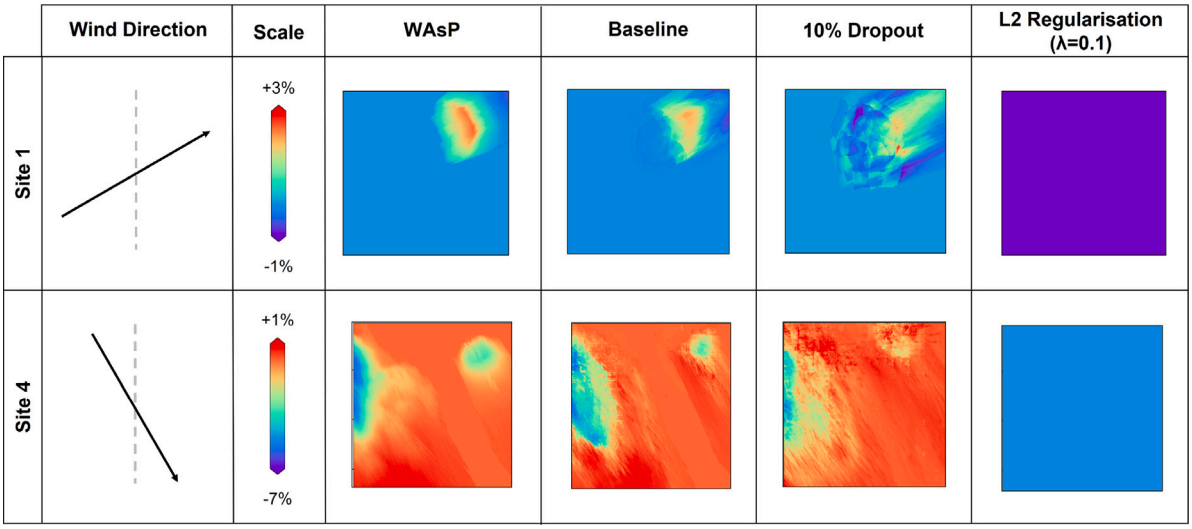

Fig. 13. Application of techniques to prevent overfitting in a GKNN model at 100 m AGL, for Site 1 (top) and Site 4 (bottom), from (left–right): WAsP; GKNN with no dropout or weight regularisation; GKNN with dropout of 10%; GKNN with weight regularisation with decay factor 0.1. Speedup colour scales are based on WAsP outputs.

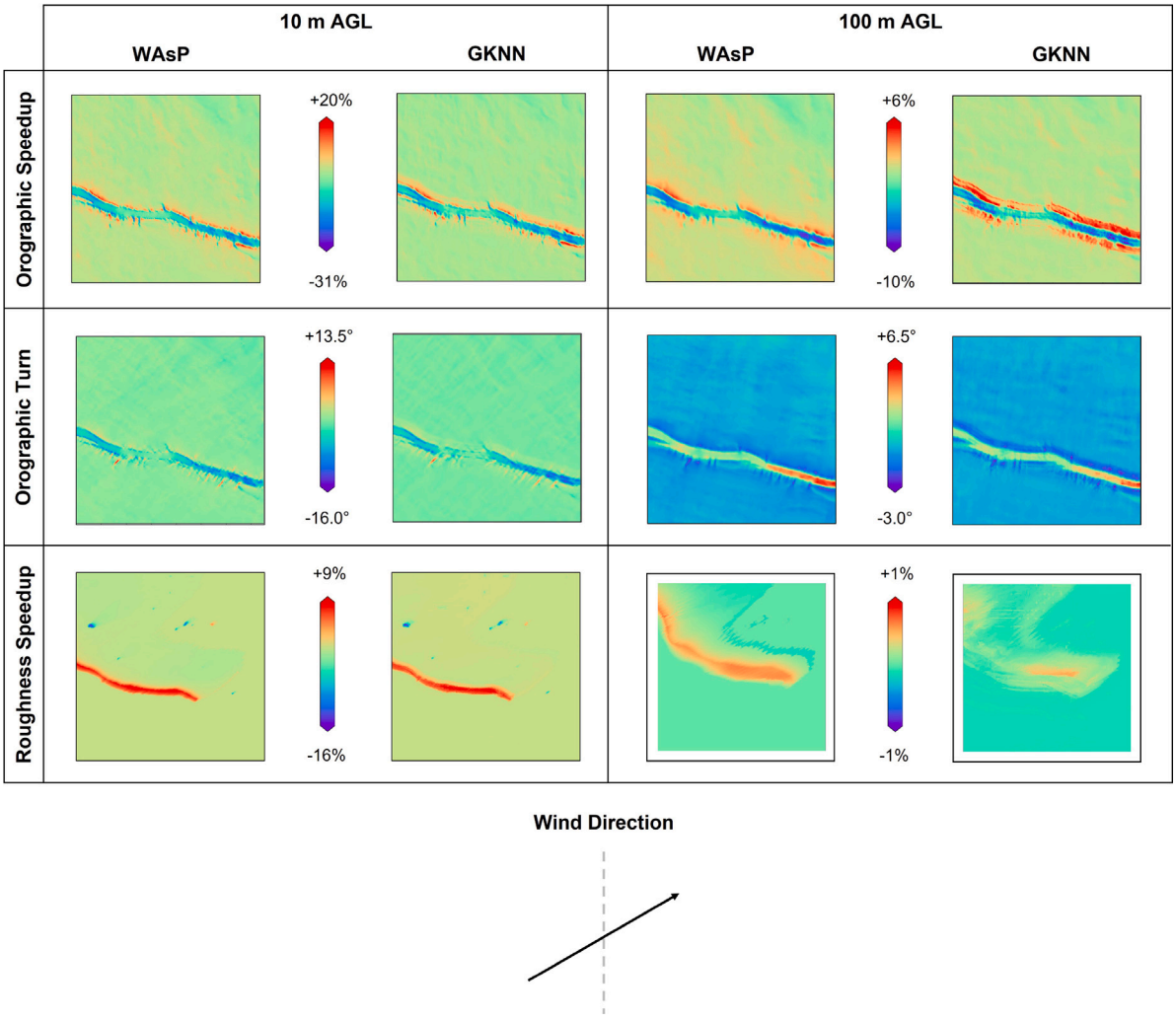

Fig. 14. Results from inference on the final GKNN models on Site 13. Showing (left–right): WAsP calculated output at 10 m AGL; GKNN prediction at 10 m AGL; WAsP calculated output at 100 m AGL; GKNN prediction at 100 m AGL. Output variables plotted are (top–bottom): orographic speedup; orographic turn; roughness speedup. All speedup values are in % speedup; all turn values are in ° clockwise; speedup and turn colour scales are based on WAsP outputs.

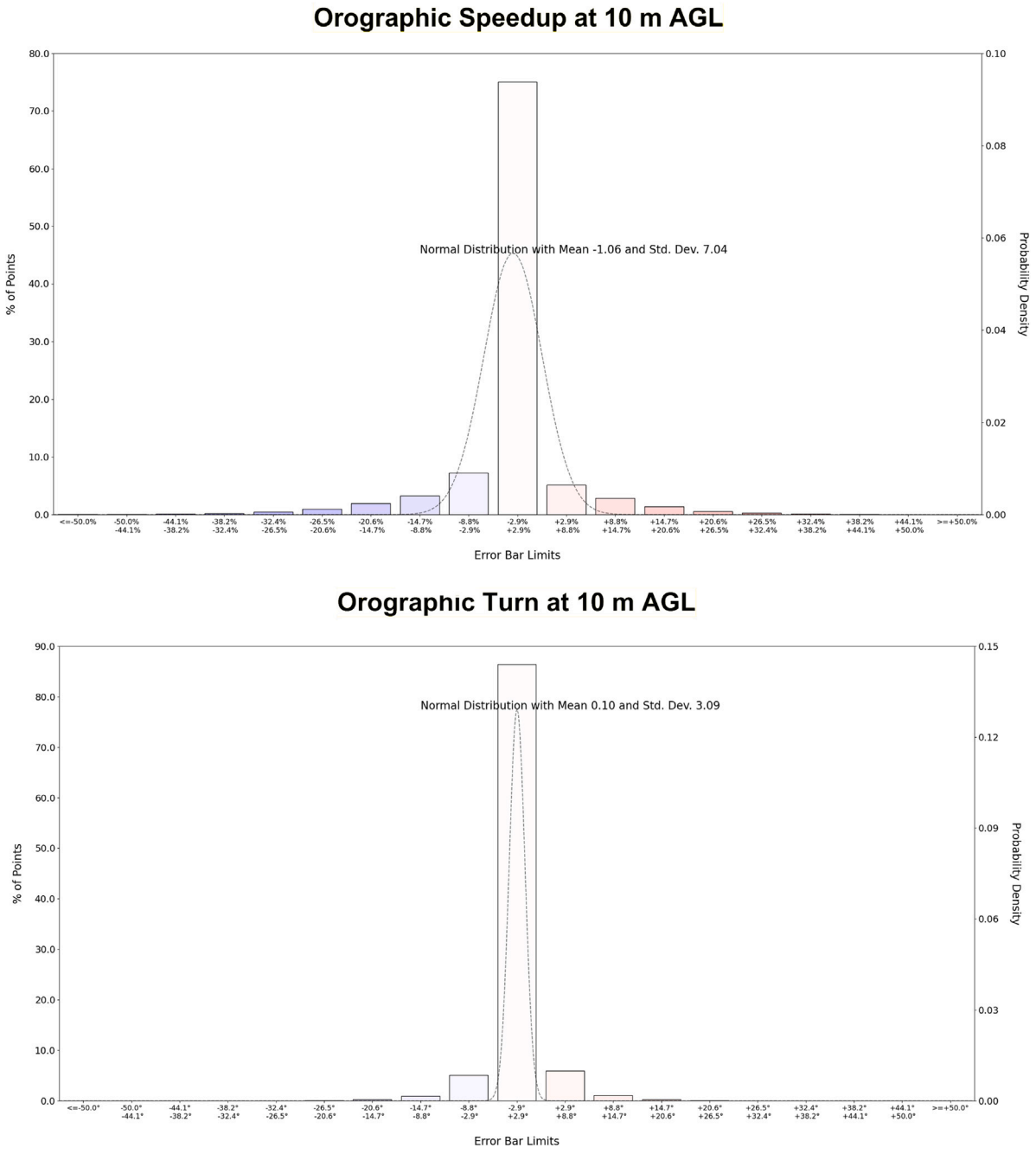

Fig. 15. Distributions of errors in the GKNN predictions over Sites 12–14, for (top) orographic speedup at 10 m AGL and (bottom) orographic turn at 10 m AGL. All speedup values are in % speedup; all turn values are in ° clockwise. Bar colours represent the degree of over- (red) or under-prediction (blue), with more intense colours for larger errors. (For interpretation of the references to colour in this figure legend, the reader is referred to the web version of this article.)

speedup and turn, the GKNN outputs were a good match overall to the WAsP calculated data over the various terrains, with the shapes and scales of the majority of speedup and turn values close to the ground truth. As outlined in Section 5.1, the orographic speedup surrogate models performed well where the speedup was closely correlated to the elevation or its gradient (e.g. decreases in speed through valleys as shown in Fig. 14 for both heights), but could not match the most extreme changes in speed. Both the orographic speedup and turn surrogate models incorrectly predicted large changes in the wind speed and direction respectively over the area of high roughness in the otherwise flat Site 14 (see Fig. A.14); this behaviour was also seen in Site 4 of the validation data, e.g. Fig. 5. Despite the large maximum and minimum errors given in Table 5 for orographic speedup and turn at 10 m AGL, Fig. 15 shows that these are outliers and that the majority of errors are very small. The predictions for the roughness speedup over these three new sites were very promising at both 10 m and 100 m AGL, with the MAE decreasing in both cases compared to the validation sites. This is unusual, and likely due to the (unintentional) choice of sites which contain mostly uniform roughness, with small, well-defined areas of differing roughness lengths (e.g. the valley shown in Fig. A.13) at which the surrogate models excelled. Despite this, there is still evidence that the GKNNs have not fully learned how to apply large areas of "roughness persistence", as seen in Fig. 14 at 100 m AGL.

6. Conclusions

In this work, grid-based machine learning techniques were used to create data-driven models for the calculation of terrain-induced wind velocity changes, with the aim of emulating the WAsP orographic and roughness sub-models at two distinct heights above ground. Convolutional Neural Networks, while successful as surrogate models for other fluid dynamics simulations, proved to be unsuitable for calculating the orographic and roughness speedups. Hence, a *Grid-Kernel Neural Network* method was developed here, which takes points from a given kernel size and pattern (analogous to a filter in a CNN) over various terrain data maps (as inputs) and speedup or turn maps (as outputs).

Separate GKNNs were created and trained for the orographic speedup, orographic turn and the roughness speedup, at heights of 10 m and 100 m AGL. The GKNNs for orographic speedup produced outputs which closely matched the WAsP speedup maps at both heights, with MAE of 3.7% and 1.6% speedup at 10 m and 100 m AGL respectively. The surrogate models performed best where the form of the speedup was closely related to the input terrain (e.g. air flowing through valleys), while some small areas of speedup were not captured in the predictions. Using GKNNs as surrogate models for orographic turn showed similar results, and correlated well to the equivalent WAsP values over most sites at both heights (with MAE of 1.4° at 10 m AGL and 0.4° at 100 m AGL), particularly where there were clear influences of the terrain on the turn values. In WAsP, the effect of roughness transitions on the wind speed propagates vertically upward with downstream distance, unlike orography-induced changes which are influenced by close terrain features. This made creating GKNN models for roughness speedup more challenging, as different optimal kernel sizes were found for the two different heights; the final models both had MAE of less than 1% speedup. While the GKNNs did learn to apply roughness speedups downstream of transitions, there were some sites over which the GKNN produced poor predictions at 100 m AGL, with no easily discernible reason for this other than possible overfitting.

Future work could focus on integrating the predictions from the GKNNs for three separate output variables and different heights into a single wind resource calculation at a user-specified height AGL, possibly by interpolating between defined heights. More work could also be done on the prevention of overfitting in the models, as they showed signs of this issue, potentially through training with more sites, additional input variables, or further investigation into dropout and regularisation. Finally, given the aim of this work was to produce a "proof-of-concept" data-driven surrogate wind resource model, the next step would be to apply the novel GKNN technique to CFD wind resource data.

CRediT authorship contribution statement

Helen Sheehan: Methodology, Software, Investigation, Writing – original draft, Writing – review & editing, Visualization. **Elizabeth Traiger:** Conceptualization, Methodology, Data curation, Writing – review & editing. **Daniel Poole:** Methodology, Supervision, Writing – review & editing. **Lars Landberg:** Conceptualization, Methodology, Resources, Supervision, Writing – review & editing.

Declaration of competing interest

The authors declare that they have no known competing financial interests or personal relationships that could have appeared to influence the work reported in this paper.

Data availability

The data that has been used is confidential.

Acknowledgements

The authors would be like to thank both Dr. Paul Harper, Lecturer at University of Bristol, and Prof. Ervin Bossanyi, Senior Principal Researcher at DNV and Visiting Professor at University of Bristol, for their enduring academic support through this research.

Appendix A. Terrain maps

See Figs. A.1–A.14.

Appendix B. Additional validation results

B.1. Orographic speedup

See Fig. B.1.

B.2. Orographic turn

See Fig. B.2.

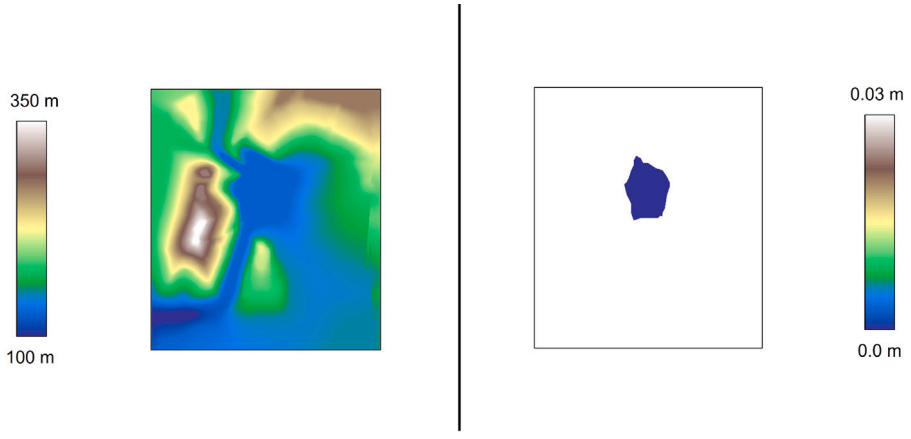

Fig. A.1. Elevation (left) and roughness (right) for Site 1 (Waspdale).

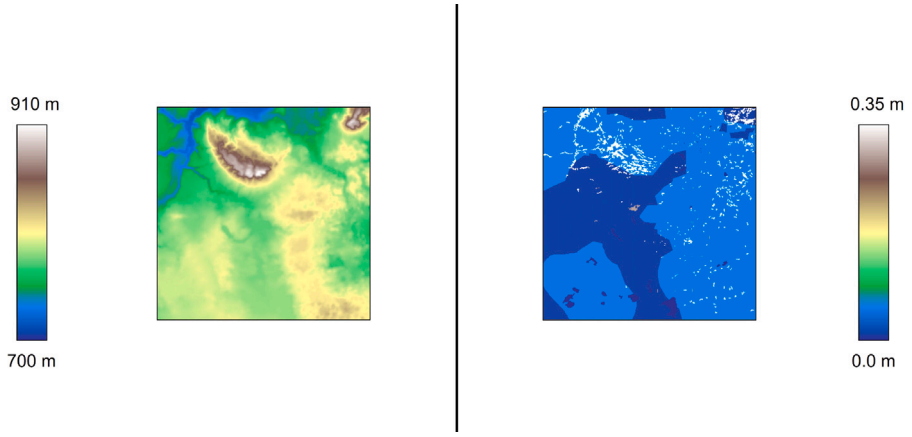

Fig. A.2. Elevation (left) and roughness (right) for Site 2.

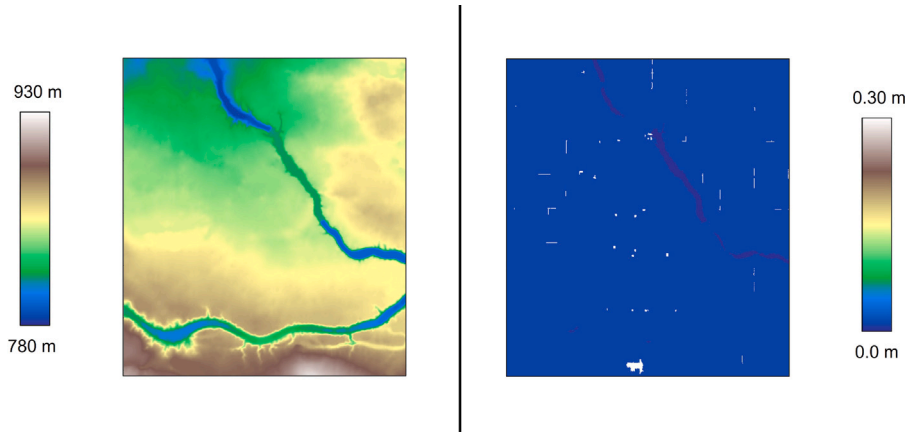

Fig. A.3. Elevation (left) and roughness (right) for Site 3.

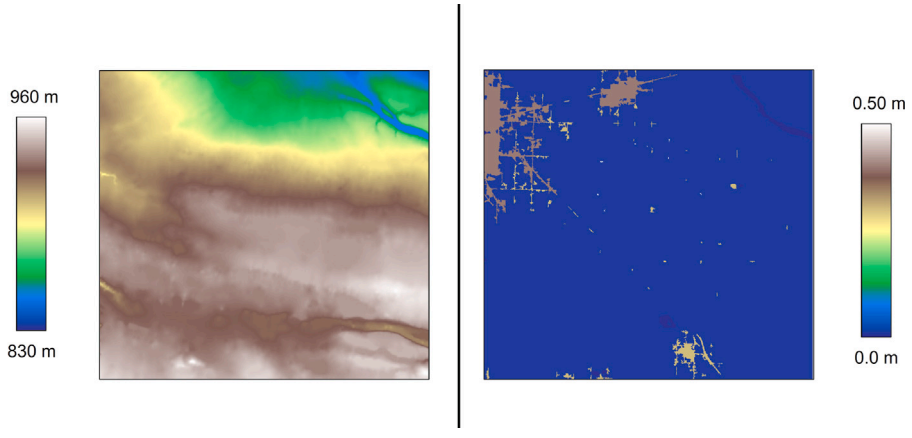

Fig. A.4. Elevation (left) and roughness (right) for Site 4.

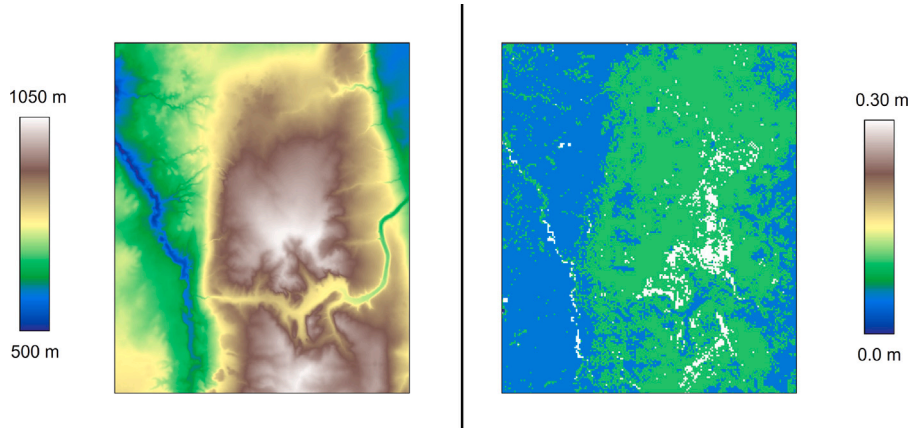

Fig. A.5. Elevation (left) and roughness (right) for Site 5.

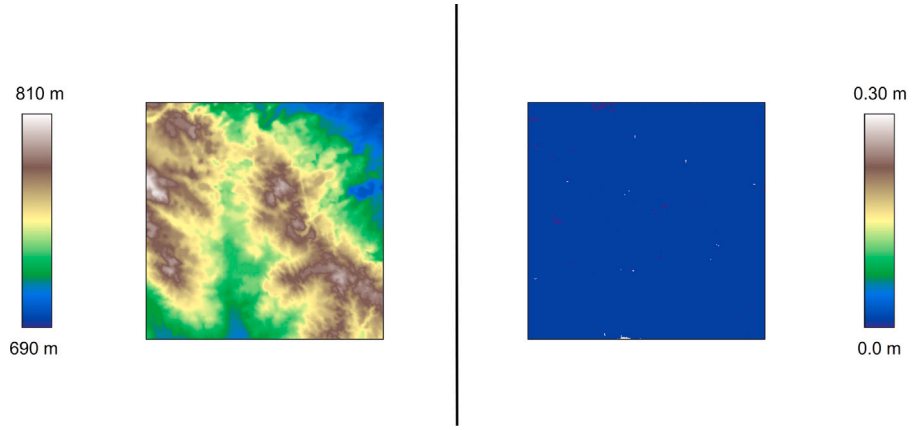

Fig. A.6. Elevation (left) and roughness (right) for Site 6.

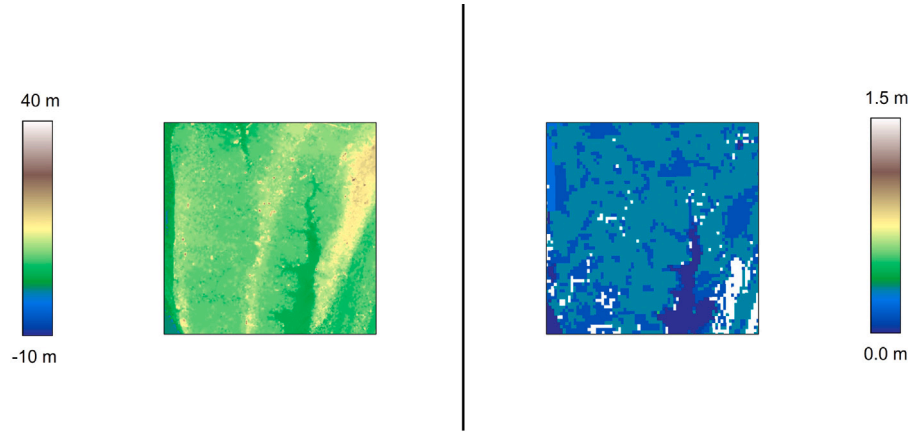

Fig. A.7. Elevation (left) and roughness (right) for Site 7.

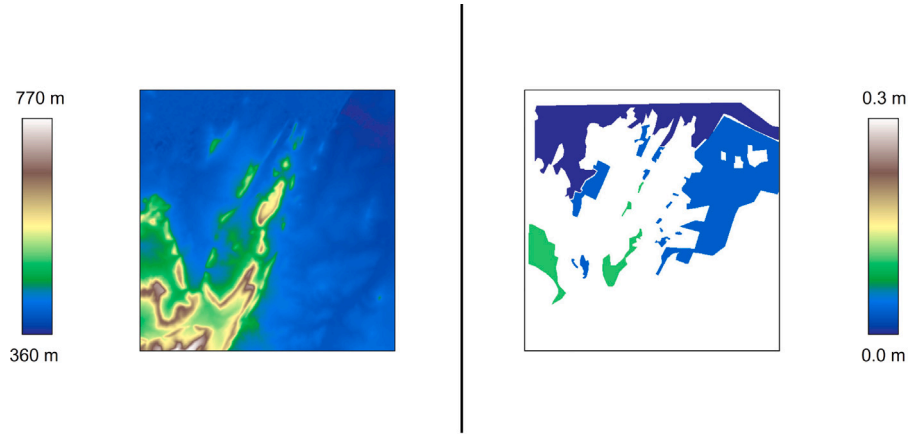

Fig. A.8. Elevation (left) and roughness (right) for Site 8.

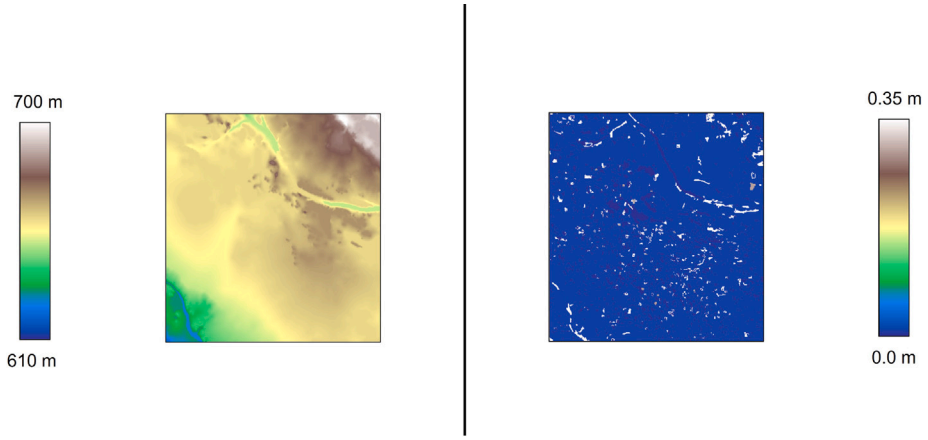

Fig. A.9. Elevation (left) and roughness (right) for Site 9.

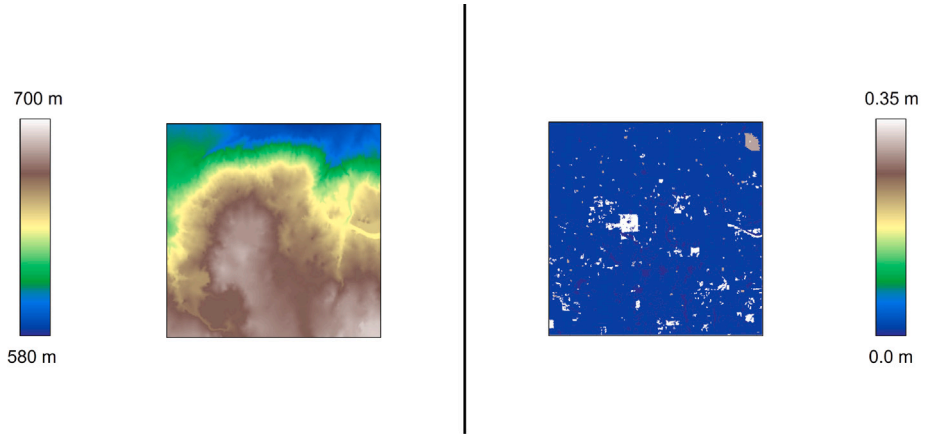

Fig. A.10. Elevation (left) and roughness (right) for Site 10.

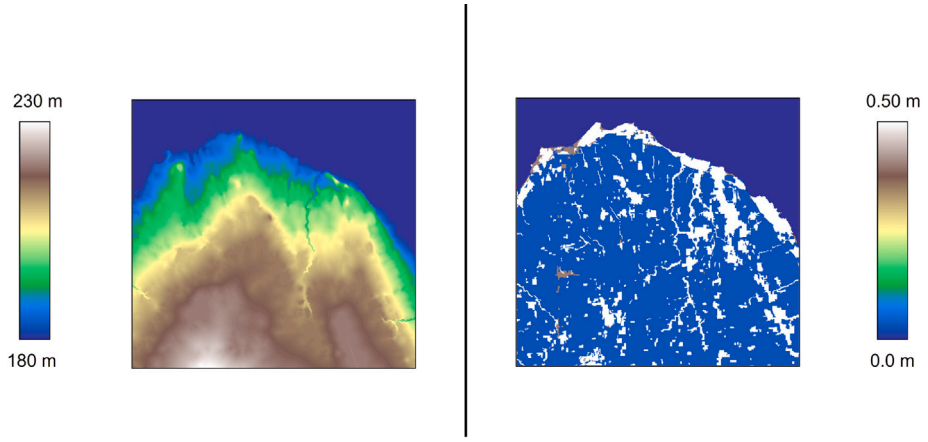

Fig. A.11. Elevation (left) and roughness (right) for Site 11.

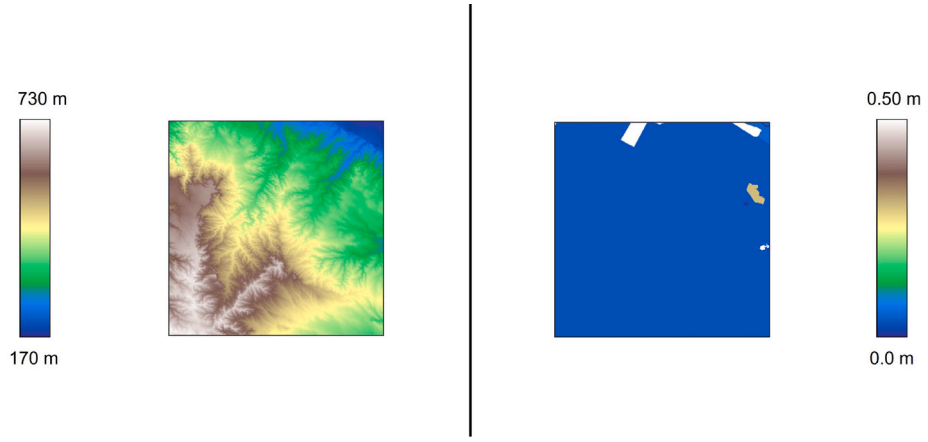

Fig. A.12. Elevation (left) and roughness (right) for Site 12.

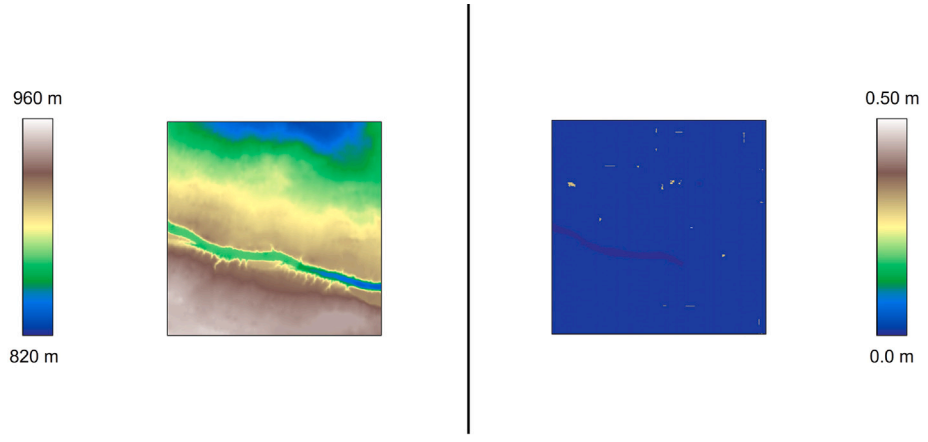

Fig. A.13. Elevation (left) and roughness (right) for Site 13.

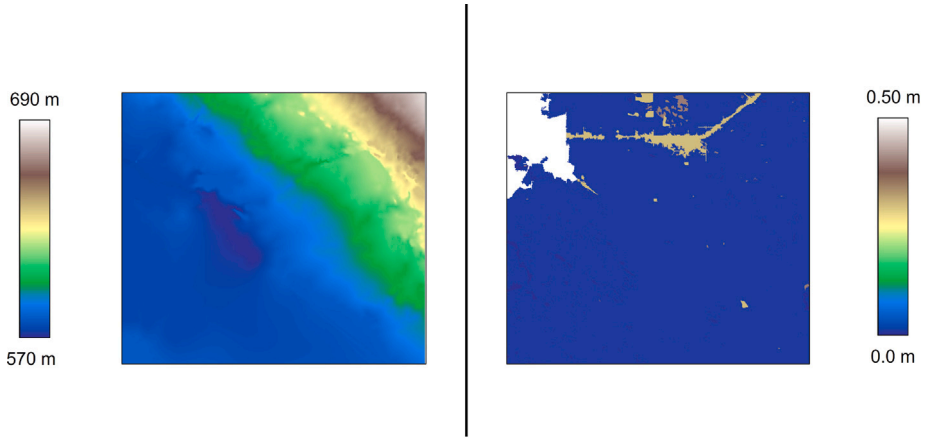

Fig. A.14. Elevation (left) and roughness (right) for Site 14.

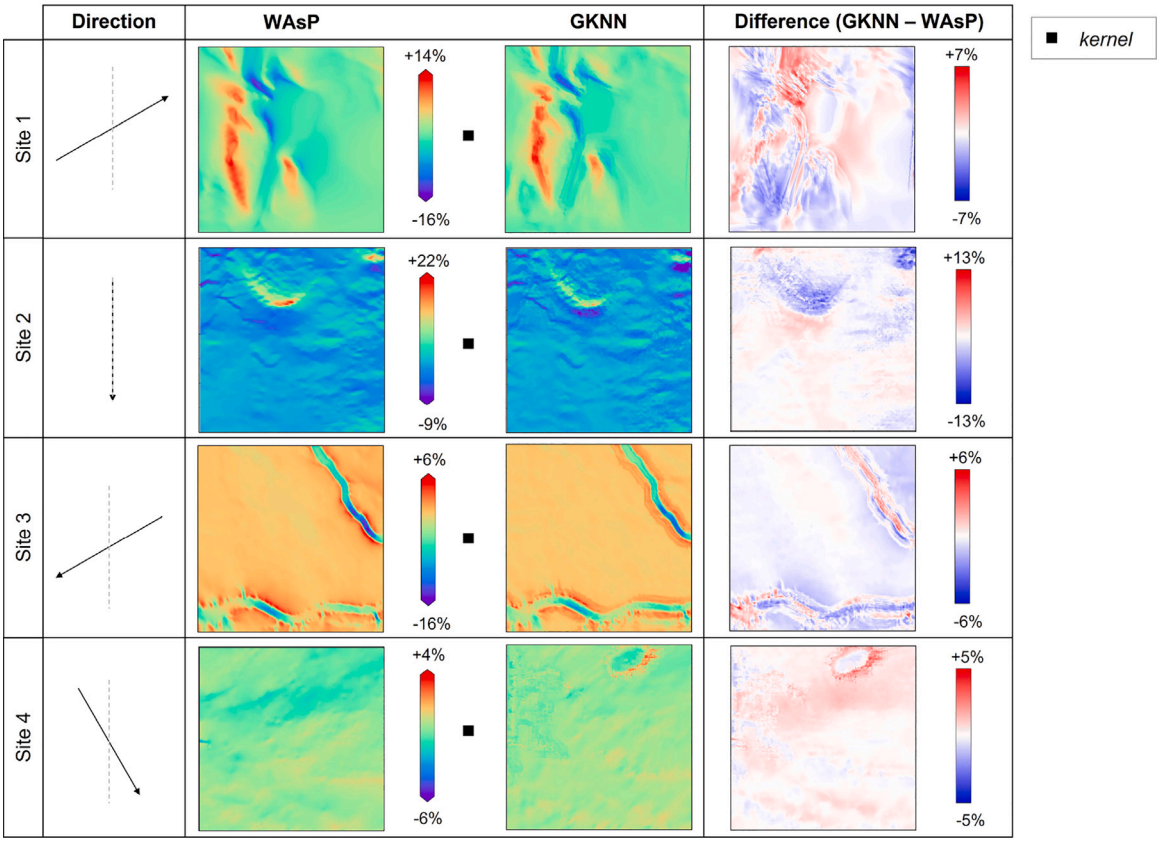

Fig. B.1. Results from the final GKNN model for predicting orographic speedup at 100 m AGL; for (top–bottom) Sites 1–4, shows (left–right): WAsP calculated speedup; GKNN predicted speedup; difference (GKNN-WAsP). All speedup and difference values are in % speedup; speedup colour scales are based on WAsP outputs.

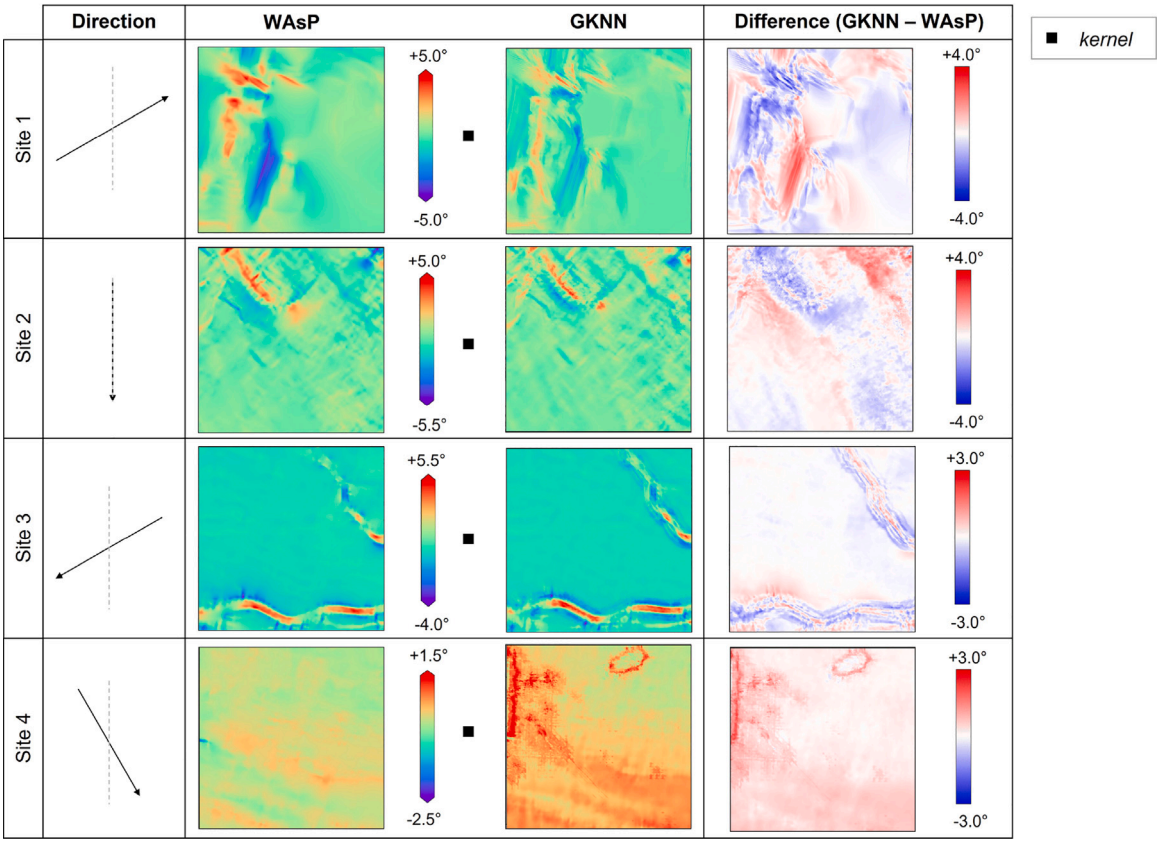

Fig. B.2. Results from the final GKNN model for predicting orographic turn at 100 m AGL; for (top–bottom) Sites 1–4, shows (left–right): WAsP calculated turn; GKNN predicted turn; difference (GKNN-WAsP). All turn and difference values are in °; turn colour scales are based on WAsP outputs.

References

Bhatnagar, S., Afshar, Y., Pan, S., Duraisamy, K., Kaushik, S., 2019. Prediction of aerodynamic flow fields using convolutional neural networks. Comput. Mech. 64, 525–545.

Bleeg, J., Purcell, M., Ruisi, R., Traiger, E., 2018. Wind farm blockage and the consequences of neglecting its impact on energy production. Energies 11, 1609.

Bowen, A.J., Mortensen, N.G., 2004. WAsP Prediction Errors Due to Site Orography. Risoe-R No. 995(EN), Forskningscenter Risoe, Denmark.

Byrne, R., Hewitt, N.J., Griffiths, P., MacArtain, P., 2021. A comparison of four microscale wind flow models in predicting the real-world performance of a large-scale peri-urban wind turbine, using onsite LiDAR wind measurements. Sustain. Energy Technolo. Assess. 46.

Donadio, L., Fang, J., Porté-Agel, F., 2021. Numerical weather prediction and artificial neural network coupling for wind energy forecast. Energies 14.

DTU Wind Energy, 2022. WAsP. URL: https://www.wasp.dk/, Last accessed: 08/07/2022.

Frandsen, S., Barthelmie, R., Pryor, S., Rathmann, O., Larsen, S., Højstrup, J., Thøgersen, M., 2006. Analytical modelling of wind speed deficit in large offshore wind farms. Wind Energy 9, 39–53.

van der Hoek, D., Doekemeijer, B., Andersson, L.E., van Wingerden, J.-W., 2020. Predicting the benefit of wake steering on the annual energy production of a wind farm using large eddy simulations and Gaussian process regression. J. Phys. Conf. Ser. 1618.

Howland, M.F., Dabiri, J.O., 2019. Wind farm modeling with interpretable physics-informed machine learning. Energies 12, 2716.

Ioffe, S., Szegedy, C., 2015. Batch normalization: Accelerating deep network training by reducing internal covariate shift. arXiv:1502.03167.

Isola, P., Zhu, J.-Y., Zhou, T., Efros, A.A., 2016. Image-to-image translation with conditional adversarial networks. arXiv:1611.07004.

Jackson, P.S., Hunt, J.C.R., 1975. Turbulent wind flow over a low hill. Q. J. R. Meteorol. Soc. 101, 929–955.

Jensen, N.O., 1983. A Note on Wind Generator Interaction. Risø-M No. 2411, Risø National Laboratory.

Kareem, A., 2020. Emerging frontiers in wind engineering: Computing, stochastics, machine learning and beyond. J. Wind Eng. Ind. Aerodyn. 206.

Kheirabadi, A.C., Nagamune, R., 2019. A quantitative review of wind farm control with the objective of wind farm power maximization. J. Wind Eng. Ind. Aerodyn. 192, 45–73.

Ladický, L., Jeong, S., Solenthaler, B., Pollefeys, M., Gross, M., 2015. Data-driven fluid simulations using regression forests. ACM Trans. Graph. 34, 1–9.

Lalonde, E.R., Vischschraper, B., Bitsuamlak, G., Dai, K., 2021. Comparison of neural network types and architectures for generating a surrogate aerodynamic wind turbine blade model. J. Wind Eng. Ind. Aerodyn. 216.

Lee, D., Jeong, S.Y., Kang, T.H.-K., 2022. Consideration of terrain features from satellite imagery in machine learning of basic wind speed. Build. Environ. 213, 108866.

Lee, S., You, D., 2019. Data-driven prediction of unsteady flow over a circular cylinder using deep learning. J. Fluid Mech. 879, 217–254.

Mortensen, N.G., 2016. Wind resource assessment using the WAsP software (DTU Wind Energy E-0135). DTU Wind Energy E No. 0135, Technical University of Denmark.

Navarro Diaz, G.P., Saulo, A.C., Otero, A.D., 2019. Wind farm interference and terrain interaction simulation by means of an adaptive actuator disc. J. Wind Eng. Ind. Aerodyn. 186, 58–67.

Pfaff, T., Fortunato, M., Sanchez-Gonzalez, A., Battaglia, P.W., 2020. Learning mesh-based simulation with graph networks. arXiv:2010.03409.

Quiroga-Novoa, P., Cuevas-Figueroa, G., Preciado, J.L., Floors, R., Peña, A., Probst, O., 2021. Towards better wind resource modeling in complex terrain: A k-nearest neighbors approach. Energies 14, 4364.

Raissi, M., Perdikaris, P., Karniadakis, G.E., 2019. Physics-informed neural networks: A deep learning framework for solving forward and inverse problems involving nonlinear partial differential equations. J. Comput. Phys. 378, 686–707. http://dx.doi.org/10.1016/j.jcp.2018.10.045.

Regan, T., Beale, C., Inalpolat, M., 2017. Wind turbine blade damage detection using supervised machine learning algorithms. J. Vib. Acoust. 139.

Ronneberger, O., Fischer, P., Brox, T., 2015. U-Net: Convolutional networks for biomedical image segmentation. arXiv:1505.04597.

Sharma, R., Shikhola, T., Kohli, J.K., 2020. Modified fuzzy Q-learning based wind speed prediction. J. Wind Eng. Ind. Aerodyn. 206.

Sheehan, H.M., 2022. Machine Learning for Wind Flow Modelling: Using Grid-Based Neural Networks to Capture Wind Flow Changes Over Terrain (MSc Thesis). University of Bristol, Brisol, UK, https://research-information.bris.ac.uk/ws/portalfiles/portal/325066422/Final_Copy_2022_06_06_Sheehan_H_M_MScR.pdf.

Song, M.X., Chen, K., He, Z.Y., Zhang, X., 2014. Wind resource assessment on complex terrain based on observations of a single anemometer. J. Wind Eng. Ind. Aerodyn. 125, 22–29.

Thuerey, N., Weißenow, K., Prantl, L., Hu, X., 2020. Deep learning methods for Reynolds-averaged Navier-Stokes simulations of airfoil flows. AIAA J. 58, 25–36.

Troen, I., 1990. A high resolution spectral model for flow in complex terrain. 9. Symposium on turbulence and diffusion, American Meteorological Society, pp. 417–420.

Troen, I., Lundtang Petersen, E., 1989. European Wind Atlas. Risø National Laboratory.

Walmsley, J.L., Troen, I., Lalas, D.P., Mason, P.J., 1990. Surface-layer flow in complex terrain: Comparison of models and full-scale observations. Bound. Layer Meteorol. 52, 259–281.

Zhang, J., Zhao, X., 2021. Spatiotemporal wind field prediction based on physics-informed deep learning and LIDAR measurements. Appl. Energy 288.